Order Number 9521291

# Detection of buried objects using thermal infrared imaging

Li, Ping, Ph.D.

City University of New York, 1995



U·M·I
300 N. Zeeb Rd.
Ann Arbor, MI 48106

# DETECTION OF BURIED OBJECTS USING THERMAL INFRARED IMAGING

BY

PING LI

A dissertation submitted to the Graduate Faculty in Engineering

in partial fulfillment of the requirements for the degree of

Doctor of Philosophy

The City University of New York

1995

This Manuscript has been read and accepted for the Graduate Faculty in Engineering in satisfaction of the dissertation requirements for the degree of Doctor of Philosophy.

12/14/94

Date

Chair of Examining Committee

Professor Samir A. Ahmed

12/14/94

Date

Executive Officer

Professor Gerald Lowen

Professor Mohamed Ali

Professor Joseph Barba

Professor Fred Moshary

Professor Leonid Roytman

Professor Tarek N. Saadawi

Dr. Demetri Kokkinos

Supervisory Committee

The City University of New York

**Abstract**

# DETECTION OF BURIED OBJECTS USING THERMAL INFRARED IMAGING

by Ping Li

Adviser: Professor Samir Ahmed

Thermal infrared images of the surface of the ground provide information about the near surface physical state of geologic materials. So, if an object is buried close to the surface of the ground, the temperature contours will show on the thermal infrared image, especially when surface temperatures changes or the radiation flux on the surface changes. This is due to a buried object's different thermal properties when they transmit their thermal imprints to the immediate surface of the ground differently than the other area. The advantage of thermal infrared imaging techniques is that they yield information on the depth and topographical shape as well as the material composition of a buried object and thus have great potential for location and highly accurate identification of the object.

In this work, we seek to systematically examine, both theoretically and experimentally, all the factors that characterize the surface thermal imprints and their relationships to (i) the buried objects and their geometric and thermal characteristics, (ii) their distance from the surface and the soil medium in which they are buried, and (iii) the surrounding heating and cooling of the surface. Based on a comprehensive examination and understanding of these factors and the possibilities they present, we set up a system for close-in detection of select buried objects.

We discussed the use of the diurnal solar cycle and an artificial step function radiation heating and cooling of a sand surface to detect the presence of buried objects. The mathematical models of temperature distribution on the surface of the ground buried with a semi-infinite and finite object underneath, heated and cooled by either a diurnal solar cycle or an artificial step function radiation source were studied and developed.

Numerical simulations and experimental works characterizing the surface thermal imprints of the different materials of objects with different buried depth were carried out showing the capabilities of thermal infrared imaging for detecting the buried objects. The further works of data and image processing demonstrated the capability of both further enhancement in sensitivity and increased detection speed.

## Acknowledgments

I would like to express my gratitude to my mentor, Professor Samir Ahmed, Dean Gerald Lowen, and the members of the examining committee, Professor Mohamed Ali, Professor Joseph Barba, Professor Fred Moshary, Professor Leonid Roytman, Professor Tarek N. Saadawi and Dr. Demetri Kokkinos.

My thanks to my fellow students at the Infrared Imaging Laboratory.

To my dear parents, Xinkui Li and Roulin Liang,
my sister and brother, Li Li and Dong Li
whose patience,
great support and
understanding
encouraged me
to attain most
of my goals of this
Ph. D degree.

李苹

LI, PING

一九九四年

# Table of Contents

# I. INTRODUCTION

# Introduction

## 1.1 Introduction and background

Every object, whether it is animate or inanimate, radiates infrared energy proportional to its temperature. With the aid of thermal infrared imaging, we can look at an object and detect variations in its surface temperature with high resolution. Those variations can be interpreted to provide valuable information.

One great advantage of thermal infrared imaging is that it is a passive measurement technique. Some objects —— the sun, the stars, flames and fluorescent tubes —— radiate visible light of their own. But most things are seen only by light reflected from external sources. If no such source is available, or if the objects are buried, then we are left in the dark and see nothing. Thermal infrared imaging needs no light source, because it detects and measures the objects according to their temperature which are dependent on the amounts of infrared radiation the objects emit.

Another advantage is that thermal infrared imaging operates without physical contact. It allows rapid assessment of a situation of either white hot or frozen cool via thermal patterns and shows the operator exactly what is being measured from a safe distance. It also has a much faster response time (nanosecond vs. milliseconds) than non-contact measurement. Also —— an important point in some applications —— the non-contact principle means that the act of observing does not influence the condition of the object observed.

All those advantages enable thermal infrared imaging technique to play so important a role in science, technology and industry. In science, thermal infrared imaging is aiding the exploration of unknown territory and is used to study the high-temperature aerodynamic conditions encountered by vehicles re-entering earth's atmosphere, a key

factor in the development of the Space Shuttle. The applications of thermal infrared imaging in industries are: 1) product development. One example is electronics testing to look beneath the surface of a hybrid permits detection of defects in materials, processes or workmanship, and to detect faults in printed circuit boards; 2) condition monitoring, such as maintenance inspection of switch-gear at electric power distribution substations, flat roof moisture detection, steam lines and steam traps monitoring; and 3) process monitoring and control where temperature is a useful indicator of whether the operation is proceeding as it should. In medically oriented investigation, the technique is used to assist in a variety of projects on the pathogenesis, treatment, and management of such major cold injuries as trench foot, frostbite, and hypothermia. The versatility of thermal infrared imaging is truly impressive. Research and development applications for this technique are increasing at a rapid rate.[ 1, 2, 3, 4, 5, 6 ].

We are more interested in using thermal infrared imaging to detect buried objects.

It is known that if an object is buried close to the soil surface, the surface above the buried object exhibits a thermal contrast to the surrounding soil, especially when the surface temperature changes or the radiation flux on the surface changes. This change results from the different thermal properties of a buried object which will transmit its thermal imprints to the soil surface differently than that of non-disturbed soil. Since thermal infrared imaging technique is able to identify surface temperature patterns, the object under the surface of the soil can be detected. Objects made of different material and buried at different depths are identified by their unique thermal properties. [ 18, 19, 20, 23, 24, 25 ].

Theoretical studies and experimental measurements of the effects of buried land mines on soil surface temperature distributions were done in the late 1950s and 1960s [7]·

In 1953 [16], Jaeger developed a technique to find a relationship between surface heat flux and surface temperature for periodic heating of a semi-infinite solid. This relationship had been used by Watson, in 1971 [13], in remote sensing study to derive a

thermal model for exploring the diurnal temperature behavior of several rock types and predicting times for optimum contrast among them. And in 1973 [15], Watson further used the technique to the periodic heating of a layer over a semi-infinite solid. His numerical example showed the limitation of layer thickened at which an insulation layer either has no discernible effect or completely masks the underlying material. Watson's model had been used as a guide in geologic application, to detect the mineral field covered by soil or lichen.

Recent advances in infrared detectors and closed cycle cryo-cooler technology have lead to a new generation of moderately priced, rugged portable cameras operating in the desirable long (8-12 micrometer) wavelength range where the solar interference is considerable less than the short (3-5 micrometer) wavelength range. Thus, these cameras are ideal for imaging ambient temperature (the radiation of black body in 8-12 micrometer is approximately $5\times10^{-3}Wcm^{-2}\mu m^{-1}$ at 30° C) objects with a resolution of better than 0.1° C. These advances have lead to renewed interest in the application of infrared imaging to the detection and identification of buried objects [ 8, 9, 10, 11 ].

One of the most important experiments of detecting buried objects was conducted in 1990 [11].The experiment observed and examined a land-mine's thermal images by using a vehicle mounted anti-vehicular mine detection system, which comprised a gasoline fired burner that heated a surface metal plate held parallel and close to the soil surface, and an infrared camera mounted at the opposite end of the vehicle that scanned the soil surface 3 to 5 seconds after the metal plate passed the soil surface. A temperature difference on the surface of soil indicated an object buried beneath the surface. The approach of this experiment was to use artificial heating source instead of periodic solar heating source to detect the buried objects with a finite size. So the detection could be carried at any time after heating source acted and be controlled by the operators. At the same time, the observation time could be shorter than by using periodic solar heating source. Except for the inefficiency of the heating source, the results clearly indicated that

the thermal infrared imaging technique could be used to detect a buried finite object with an artificial heating source.

But the problem of how to increase the accuracy of detection and decrease "false alarms" under any condition still remained. Besides, in order to extract information obtained from thermal infrared images, a suitable mathematical model is required which relates the relationship of the surface temperature and artificial heating flux on the surface to a finite object buried under soil.

We saught to systematically examine, both theoretically and experimentally, all the factors that characterize the surface thermal imprints and their relationships to: ( i ) the buried objects and their geometric and thermal characteristics, ( ii ) their distance from the surface and the soil medium in which they are buried, and ( iii ) the surrounding heating and cooling of the surface. Based on a comprehensive examination and understanding of these factors and the possibilities they present, we can set up a system for close-in detection of select buried objects. The system which used an infrared camera to collect thermal infrared images, can recognize potential buried objects automatically by analyzing and processing the infrared images and their data and abstract as many features and circumstances of temperature distribution on the surface of the soil as possible.

There are two types of surface temperature change that can be considered for obtaining information on underlying objects. One is due to diurnal changes produced by solar radiation. This is a relatively slow effect, with measurable changes manifesting themselves in hours. These changes can potentially be used to detect and identify buried objects. A second set of possible effects is that due to artificial step function heating and cooling, (in our case by switching on and off an intensity of radiation equivalent to typical noonday solar heating,) is seen to cause surface temperature changes which can be used to identify and distinguish objects. In Indoor experiments, these changes can manifest themselves in minutes depending on the depth of soil above the objects.

The mathematical model for both kinds of temperature changes will be studied in Part One. Using Model 740 Thermal Infrared Imaging camera (manufactured by Inframetrics Inc. in Massachusetts), we set up our experiments. The actual results of experiments will be discussed and compared with theoretical results.

Based on the experiments we did some further works in Part Two. First, we modified our mathematical model for a finite size buried object heating with a step function radiation. Second, we studied the temperature distribution on the surface with a finite buried object. Then, we analysised the data from the thermal images in experiments.

## 1.2 Thesis statement

The thermal infrared imaging technique is based on the fact that differences in the thermal properties of objects buried close to a surface will result in temperature contours on the surface as the surface is heated or cooled by the diurnal solar cycle or by artificial means. These contours are characteristic of a buried object's shape, depth, and its thermal properties. The advantage of thermal infrared imaging techniques is that they yield information on the depth and topographical shape as well as the material composition of a buried object and thus have great potential for location and highly accurate identification of the object.

The mathematical models of temperature distribution on the surface of the ground buried with a semi-infinite and finite object underneath, heated and cooled by either a diurnal solar cycle or an artificial step function radiation source were studied and developed. Numerical simulations and experimental works characterizing the surface thermal imprints of the different materials of objects with different buried depth were carried out showing the capabilities of thermal infrared imaging for detecting the buried

objects. The further works of data and image processing demonstrated the capability of both further enhancement in sensitivity and increased detection speed

## 1.3 Thesis organization

In Chapter One, we provide a general background on the development of infrared imaging technique and the principle of using infrared imaging for detecting the buried objects. In this Chapter, we present the historical development along with typical characteristics and applications. The thesis statement and organization are included here.

In Chapter Two, we reported our first part of works. The mathematical model for infinite objects buried under ground, heated and cooled with both diurnal solar cycle and artificial step function radiation sources were discussed and developed here. The numerical simulation results were given for the different material objects buried at the different depths. The experimental set-up was discussed. The experimental studies of the temperature changes of the surface of the sand, with and without buried objects, were carried out employing diurnal solar and step function radiation excitation.

In Chapter Three based on our Part One's works and discussions, we compared the results from our mathematical models and the experimental results and modified our mathematical model for a finite size object buried under the ground. A mathematical model of the temperature distribution on the surface of the ground are also discussed in this part of the work. The further works of image and data processing were carried out.

In Chapter Four, we present the conclusions of our works. Finally we discuss topics that need further research or improvement for enhancing both the detection capability and speed.

## 1.4 References

[1] Arthur Stout, "IR Images Track Heat Sources To Make Things Smart", R & D Magazine, February, 1992.

[2] Herb Boulton, Maurice Blaes, "Thermal Image Generation and Analysis", E E Evaluation Engineering, January, 1986.

[3] Hugh Danaher, "Thermograph, Understanding the Expanded Role of Thermal Images in Production Testing", E E Evaluation Engineering, December, 1988.

[4] Hugh Danaher, "Thermal Images Show Hybrids' Defects", Electronic Packaging & Production, September, 1986.

[5] JTC-310/3210 Thermograph from JEOL Thermoviewer "Introduction"

[6] Brenda M. clark, "Keeping an Eye on Hot Sports", Circuits Manufacturing, December, 1985.

[7] S. L. Carts, Jr., "Feasibility of Land Mine Detection by Infrared Thermal Imaging," Report RR-1744, Fort Belvoir, Va., USAERDL, 25 March 1963.

[8] Dwight L. Gravitte, "Field Evaluation of Hand-Held Thermal Viewer for Mine Detection," Report 2022, Fort Belvoir, Va., USAMERDC, February 1972.

[9] Dwight L. Gravitte, "Potentials and Limitations of Thermal Images for Mine Detection," Report 2172, Fort Belvoir, Va., USAMERDC, April 1976.

[10] R. V. Nolan H.C. Egghart, "Meradcom Mine Detection Program: 1960-1980," Report 2294, Fort Belvoir, Va., USAMERDC, March 1980.

[11] IIT Research Institute, "Dragon Wagon--Feasibility Study of Land-mine Thermal Signature Enhancement," Report TR-90 (6179)-1, Fort Belvoir, Va., USAMERDC, February, 1990.

[12] Harry Keller Edmund Nawrocki, "Evaluation of Thermal Viewers for Mine Detection," Report 2526, Fort Belvoir, Va., USABRDC, May 1992.

[13] Kenneth Watson, L.P. Roan, T.V. Affiliate, "Application of Thermal Modeling in the Geologic Interpretation of IR Images", International Symposium on Remote Sensing of Environment Proceedings 8th, V.2. pp.1237, 1972.

[14] Kenneth Watson, L.P. Roan, T.V. Affiliate, "Application of Thermal Modeling in the Geologic Interpretation of IR Images", International Symposium on Remote Sensing of Environment Proceedings 7th, V.3 pp.2017-2041, 1971.

[15] Kenneth Watson, "Periodic Heating of a Layer over a Semi-Infinite Solid", Journal of Geophysical Research Vol. 78, No. 26, pp.5904-5910, September 1973.

[16] H. S. Carslaw, J. C. Jagger, "Conduction of Heat in Solids", Second edition, Oxford at the Clarendon Press.

[17] Wiely D. H. Van Groningen, G. F. Vermeij, "Geometric Reconstruction of Buried Heat Sources from a Surface Thermogram", IEEE Transactions on Pattern Analysis and Machine Intelligence, Vol. PAM-7, NO. 5, pp.610-616, September 1985.

[18] Christopher D. Elvidge, "Thermal Infrared Reflectance of Dry Plant Materials: 2.5-20.0 μm", Remote Sensing of Environment 26, pp.265-285, 1988.

[19] Micheal J. Duggin, "Discrimination of Targets from Background of Similar Temperature, Using Two-Channel Data in the 3.4-3.1 μm and 11-12 μm Regions", Applied Optics Vol. 25, No. 7, pp. 1186-1195, April 1986.

[20] R. J. P. Lyon, Eugene A. Burns, "Analysis of Rocks and Minerals by Reflected Infrared Radiation", Economic Geology, Vol. 58, 1963, pp. 274-284, 1963.

[21] Arthur E. Bymes and John R. Schott, "Correction of Thermal Imagery for Atmospheric Effects Using Aircraft Measurement and Atmospheric Modeling Techniques", Applied Optics, Vol. 25, No. 15, pp. 2563-2570, August 1986.

[22] Inframetrics Model 740 IR Imaging Radiometer "User's Menu".

[23] Robert K. Vincent, "The Potential Role of Thermal Infrared Multi-spectral Scanners in Geological Remote Sensing", Proceedings of the IEEE, Vol. 63, pp.137-147, January, 1975.

[24] Richard D. Hudson, Jacqueline W. Hudson, "The Military Applications of Remote Sensing by infrared", Proceedings of the IEEE, Vol. 63, pp.105-127, January, 1975.

[25] J. C. Jaeger, "Conduction of Heat in a Solid with Periodic Boundary Conditions, with Application to the Surface Temperature of the Moon", Proceeding Cambridge Phil. Society, 49 (2),355-359, 1953.

[26] Anne B. Kahle, "A Simple Thermal Model of the Earth's Surface for Geologic Mapping by Remote Sensing", Journal of Geophysical Research, Vol. 82, No.11, pp.1673-1680, April, 1977.

[27] Robert D. Watson, Brief Reports: "Surface-Coating Effects in Remote Sensing Measurements", Journal of Geophysical Research, Vol.75, No. 2, pp.480-484, January, 1970.

[28] Lau, S. K., Almond, D. P., and Patel, P. M., "A Qauntitative Analysis of Pulsed video Thermograghic imaging of subsurface defects", in Photoacoustic and Photothermal Phenomena II, Springer Series in Optical Sciences, Vol 69, pp522-524 (Springer-Verlag 1992).

[29] Favro, L. D., Jin H. J., Kuo P. K., Thomas, R. L. and Wang, Y. X. "Real Time Thermal Wave Tomography", in Photoacoustic and Photothermal Phenomena II, Springer Series in Optical Sciences, Vol 69, pp519-521 (Springer-Verlag 1992).

[30] Aamodt, L. C. , Maclachlan Spiecer, J, W., and J. C. Murphy, "Analysis of Characteristic Thermal Transit Times for Time-Resolved Infrared Radiometry Studies of Multilayered Coatings", J. Appl. Phys. 68, pp 6087-6098 (1990).

[31] Cielo, P. "Pulsed Photothermal Evaluation of Layered Materials", J. Appl. Phys. 56, PP 230-234 (1984).

# II. PART ONE

## Part One

### 2.1 Description of the work

In Part One, we systematically examined the thermal properties of the soil surface after an object was buried with both diurnal and step function radiation flux on the surface. The characteristics of surface temperatures affected by buried objects which we examined were: 1) the effects of the buried object on the surface; 2) the relationship between surface temperature and the depth of the buried objects; 3) the rate of temperature increase and decrease according to the different material composition of the buried objects as related to the radiation source; 4) when the heat source is removed, the length of time it takes for the temperature of soil (containing the buried object) to equal the temperature of the soil without a buried object; the rate of temperature change to reach that mutual point and the temperature of that point; the rate of temperature change and the temperature of different material objects buried at the same time interval after the radiation decrease; 5) the temperature increases and relationship between the distance of the buried object and the time interval starting at the radiation switch-on to the time that the surface temperature difference can be noticed.

First, we studied a mathematical model for the surface temperature of a layer over a semi-infinite solid resulting from steady periodic heating of a one dimensional homogeneous half space. Then we developed the mathematical model for step-function radiation heating source. The experiment to measure an incident flux on the surface of the ground from our artificial step function source ( we used four infrared lamps as our step-function source ) were carried out. Numerical calculations were applied to our test objects, which are plastic, rock and metal buried under the dry sand at different depths. Using Model 740 Thermal Infrared Imaging camera (manufactured by Inframetrics Inc.

in Massachusetts), we set up our experiments. The actual results of experiments will be discussed and compared with theoretical results.

## 2.2 Mathematical model study

### 2.2.1 The problems

The problem we had was: the buried objects are finite size and the radiation sources are a diurnal solar source or a step function artificial source. As in Figure 1-1, for simplification we assumed that a finite buried object is a cylinder, with R radius and D depth and the buried distance from the object to the ground surface is L. Theoretically, the temperature distribution on the surface can be gotten by solving these differential equations [ 12 ]:

$$\frac{\partial^2 v_1}{\partial r^2}+\frac{1}{r}\frac{\partial v_1}{\partial r}+\frac{\partial^2 v_1}{\partial z^2}-\frac{1}{k_1}\frac{\partial v_1}{\partial t}=0 \qquad 0<r<R,\ |z|<D,\ t>0 \qquad (1.1)$$

$$\frac{\partial^2 v_2}{\partial r^2}+\frac{1}{r}\frac{\partial v_2}{\partial r}+\frac{\partial^2 v_2}{\partial z^2}-\frac{1}{k_2}\frac{\partial v_2}{\partial t}=0 \qquad r>R,\ |z|>D \text{ and } z>-L,\ t>0 \qquad (1.2)$$

here, $v_1$ is the temperature of the coverage materiel and $v_2$ is the temperature of the object. The boundary conditions here will be: no contact resistance at the surface of object in z direction, (i.e. at the boundary,) the temperature remains the same on both sides. The flux from the surface of the ground should be same on both sides of the object surface $S_1$. The flux from the sides and the bottom of the object should remain the same

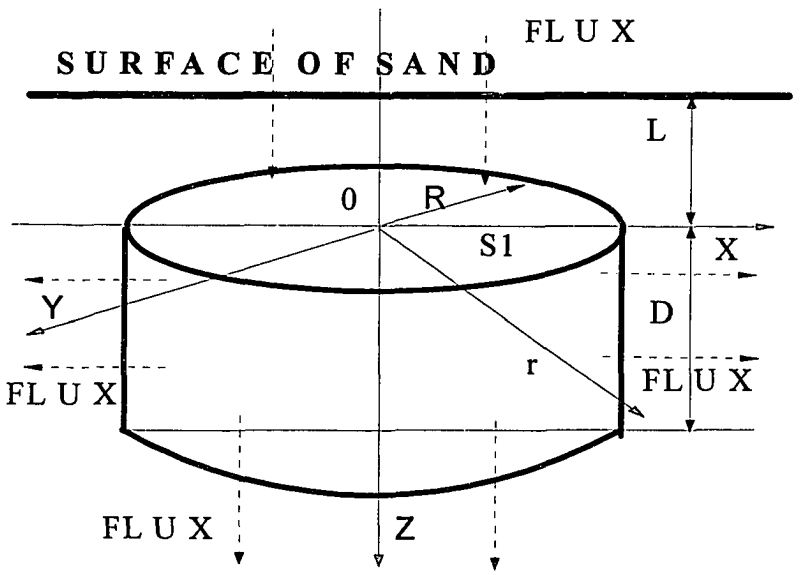


Figure 1-1
A finite object buried under the sand.

on the bounder. Radiation flux on the surface of the ground will be the sum of the flux due to artificial step function radiation and the flux due to the radiation of the sun and the sky (even in an indoor experiment).

Since the radiation flux is not constant and the side of the object cannot be assumed be insulated (i. e. the heat conduction on the sides of the object cannot be neglected), the results of the differential function will be excessively complex. We can therefore devise an alternate method to capture approximate results for explaining the distribution on the surface. First, in Part One, we set a mathematical model of a semi-finite object buried with a diurnal or a step function radiation on the surface of ground. Then, in Part Two, we modified this model for a finite sized object to get the surface temperature in the center of the object. And finally, we showed the temperature distribution on the surface of the ground.

We applied Watson's technique to our problem [8, 9, 10]. There are two reasons for us to use this technique: 1); since the size of buried object usually is much bigger than the buried distance of the object, the physical properties of the surface of ground can be simulated by the semi-finite object's model; 2); in step function radiation case, if the heating time, $T_h$, of step function is short enough, compared with the diurnal time, T, the diurnal heating model can also be used in step function heating source.

In Watson's mathematical model, the surface temperature is related by the heat flux on the surface as [10]:

$$F_n = \frac{p_2}{\sqrt{\pi T}} \sum_{r=1}^{N} v_r \theta_{n-r-1} \qquad (1.3)$$

$F_n$ is the flux into the ground in the $n^{th}$ interval. $P_2$ is the thermal inertia of the buried material. T is the period of the flux (24 hours). $V_r$ is the surface temperature of the

ground in the $r^{th}$ interval. $\theta_i$ are the coefficients required to form the relationship between the surface flux $F_n$ and the corresponding surface temperature $V_r$, which are functions of the thermal properties of the soil.

$$\theta_1 = \frac{2N^{\frac{1}{2}}}{\sigma}\left( 1+2\pi^{\frac{1}{2}} \sum_{m=1}^{\infty} \alpha^m ierfc\left( mN^{\frac{1}{2}} L' \right) \right) - \theta' \tag{1.4}$$

$$\theta_n = \frac{2N^{\frac{1}{2}}}{\sigma}\{ \left( n^{\frac{1}{2}} - 2(n-1)^{\frac{1}{2}} + (n-2)^{\frac{1}{2}} \right) + 2\pi^{\frac{1}{2}} \sum_{m=1}^{\infty} [ \alpha^m n^{\frac{1}{2}} ierfc\left( m\left( \frac{N}{n} \right)^{\frac{1}{2}} L' \right) -$$
$$2(n-1)^{\frac{1}{2}} ierfc\left( m\left( \frac{N}{n-1} \right)^{\frac{1}{2}} L' \right) +$$
$$(n-2)^{\frac{1}{2}} ierfc\left( m\left( \frac{N}{n-2} \right)^{\frac{1}{2}} L' \right) ] \} - \theta_n'$$
$$n=2,3,4,...N \tag{1.5}$$

$$\theta_n' = \frac{(Nn)^{\frac{1}{2}}}{\pi} \int_0^{\infty} \frac{e^{-x}}{x^{\frac{1}{2}}} f(x)dx \tag{1.6}$$

$$f(x) = \frac{e^{-(N-2)\frac{x}{n}} \left( 1-e^{-\frac{x}{n}} \right)^2}{x\left( 1-e^{-\frac{Nx}{n}} \right)\left[ 1+\left( \sigma^2-1 \right)\sin^2 L'\left( \frac{Nx}{n} \right)^{\frac{1}{2}} \right]} \tag{1.7}$$

An object buried underground affects the surface temperature through: 1) $F_n$; the albedo and the emissivity of the surface are effectively changed by the buried object's

thermal properties and the distance from the surface to the buried object, 2) $P_2$; thermal inertia of the buried material, 3) the set of θ's which must be computed for equation (1.3), based on the buried object's thermal properties and the distance from the surface to the buried object.

2.2.2 Basic model for diurnal function radiation

For a diurnal function radiation source, the surface flux $F_n$ in (1.3) is expressed as the sum of three terms:

$$F_n = FS_n + FA_n - FG_n \tag{1.8}$$

Where $FS_n$ is the absorbed solar flux composed of the short-wave length solar radiation (less than 4 μm) modulated by the atmospheric transmission. $FA_n$ is the absorber flux due to long-wave (greater than 4 μm) radiation from sky, which is equal to $\varepsilon T^4_{sky}$. Where $T_{sky}$ is effective sky radiance temperature; hence the absorbed flux is $\varepsilon\sigma T^4_{sky}$. $FG_n$ is reflected from the ground, which is equal to $\varepsilon\sigma V_n^4$. Here, ε is mean emssivity of the ground, σ is Stefan-Boltzmamn constant and $V_n$ is the corresponding surface temperature. This equation ignores other heat transfer mechanisms such as atmospheric conduction and convection and latent heat effects due to evaporation and/or condensation of water. The short-wave length absorbed solar flux is a function of: 1) the ground reflection in the spectral region (i.e., mostly visible and near infrared), 2) the solar declination, and 3) the local slope.

$$FS_n = f \times S_0 \times (1-A) \times M(Z) \times \cos Z' \qquad \text{in the daytime}$$

$$FS_n = 0; \qquad \text{in the nighttime} \qquad (1.9)$$

So, the heat flux into ground, which is equal to $F_n$ in (1.8) is:

$$FS_n = f \times S_0 \times (1-A) \times M(Z) \times \cos Z' + \varepsilon\sigma {T_{AD}}^4 - \varepsilon\sigma V^4$$

$$\text{in the daytime}$$

$$FS_n = \varepsilon\sigma {T_{AN}}^4 - \varepsilon\sigma V^4 \qquad \text{in the nighttime} \qquad (1.10)$$

Where:

f cloud cover factor.

$S_0$ solar constant.

A albedo of the ground.

M(Z) atmospheric transmission, approximated by

$$M(Z) = 1 - \left[ \frac{0.2}{(\cos Z)^{\frac{1}{2}}} \right].$$

Z zenith angle, $\cos(Z) = \cos\lambda\cos\delta\ (\cos\omega t + \tan\lambda\tan\delta)$.

$\lambda$ local latitude.

$\delta$ sun's declination.

t local time measured from noon.

$\omega$ diurnal angular frequency, equal to 2 /T.

$\sigma$ Stefan-boltzmamn constant.

$$\cos Z' = \cos(\lambda - d\sin\phi)\cos\delta\ \cos(\omega t + d\cos\phi) + \tan(\lambda - d\sin\phi)\tan\delta$$

Z' zenith angle modified for local slope of dip angle d and strike azimuth from north.

$T_{AD}$ effective daytime sky radiance temperature.

$T_{AN}$ effective nighttime sky radiance temperature.

$\varepsilon$ mean emissivity (spectral average) of the ground.

Based on this model our Program STF ( see Appendix B), the soil surface's diurnal temperature with various objects (plastic, cast iron and average rock) buried under the dry sand were calculated and plotted in Figure 1-2, Figure 1-3, and Figure 1-4.

The numerical example showed that as an object buried underground, the surface temperature will be different than that when nothing was buried and heated by a diurnal solar radiation. The differences of surface temperature will depend on the thermal properties of buried object and the distance from the surface to the buried object. When the buried distance increased, the temperature difference on the surface becomes smaller. If the depth of buried object is more than 10 cm, the presence of composition material cannot be detected by observing the diurnal surface temperature variation. However in ranges of less than 10 cm, as the distance of a buried object, the temperature differentials appearing on the surface above buried objects would be affected by the thermal conductivity of the buried object. For instance, a higher thermal conductivity of the object, typically associated with materials of higher thermal capacity, would mean an even lower temperature above the buried object than that of the surrounding soil as the temperature of the latter rises ( e. g. due to solar radiation). On the other hand, a lower thermal conductivity of the buried object, also typically associated with lower thermal inertia materials (such as plastic) would mean that the surface temperature above the buried object would be higher than that of soil-only area when the solar radiation increased.

The temperature change differences and the rate of temperature change due to

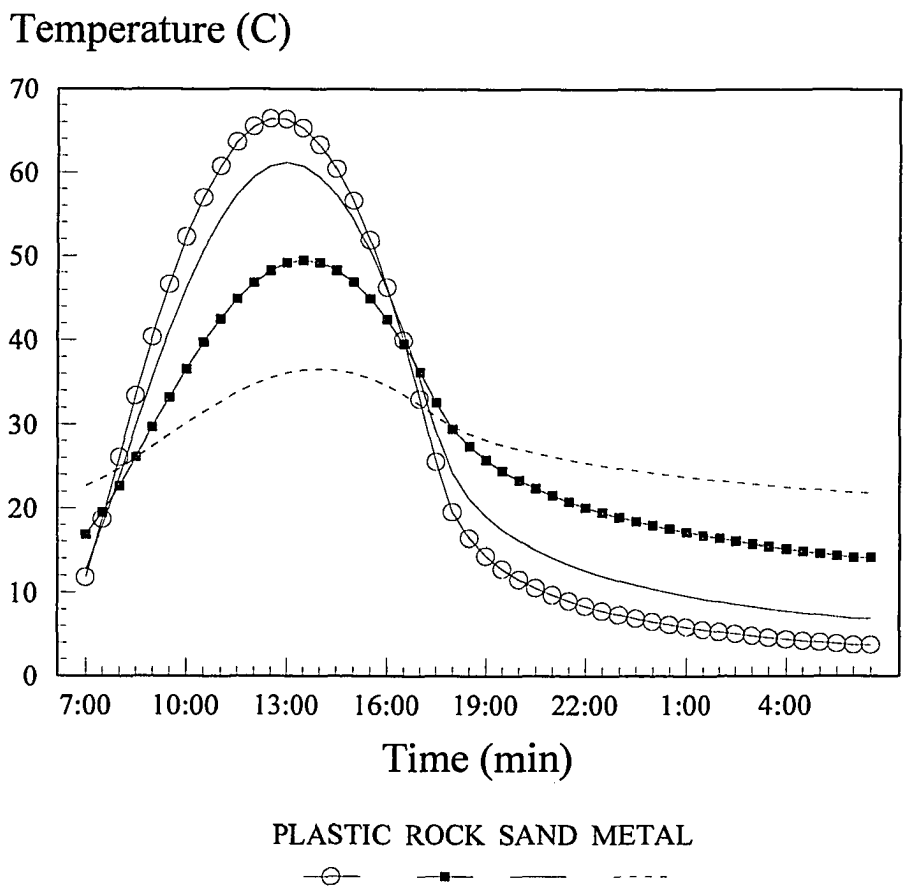


Figure 1-2
Mathematical model of diurnal solar radiation heating source with plastic, rock and metal buried under sand L = 0.3 cm.

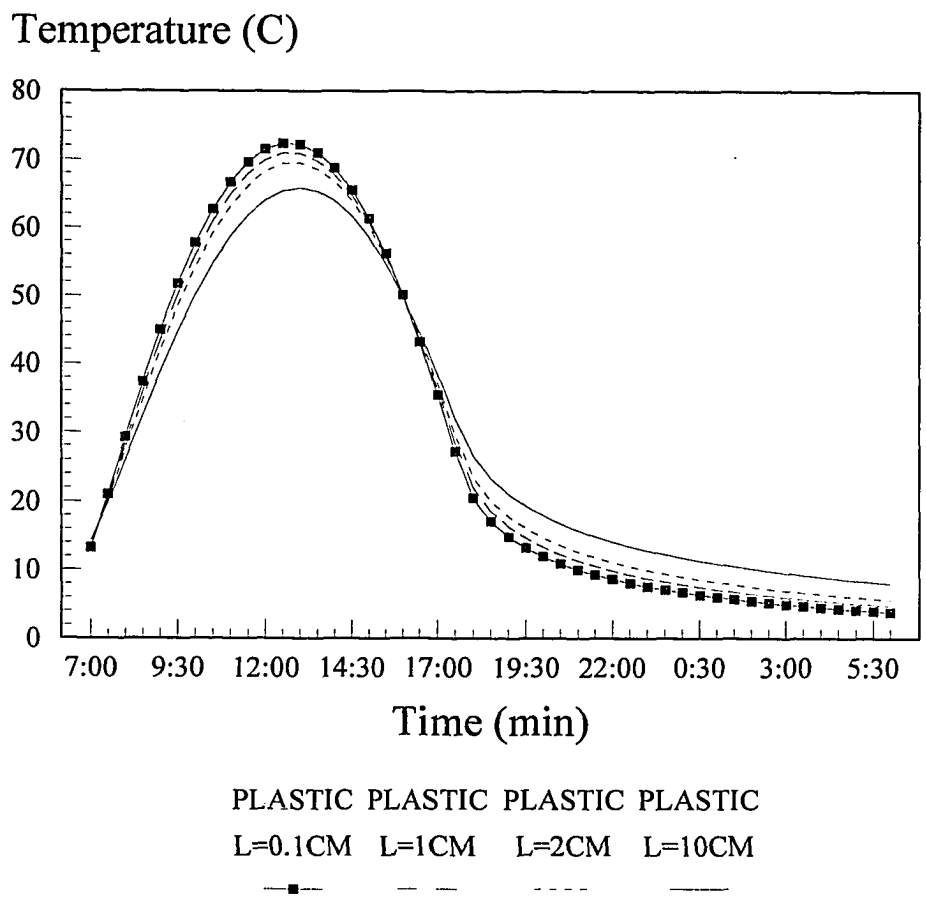


Figure 1-3
Mathematical model of diurnal solar radiation heating source with a plastic object buried at different depths under sand.

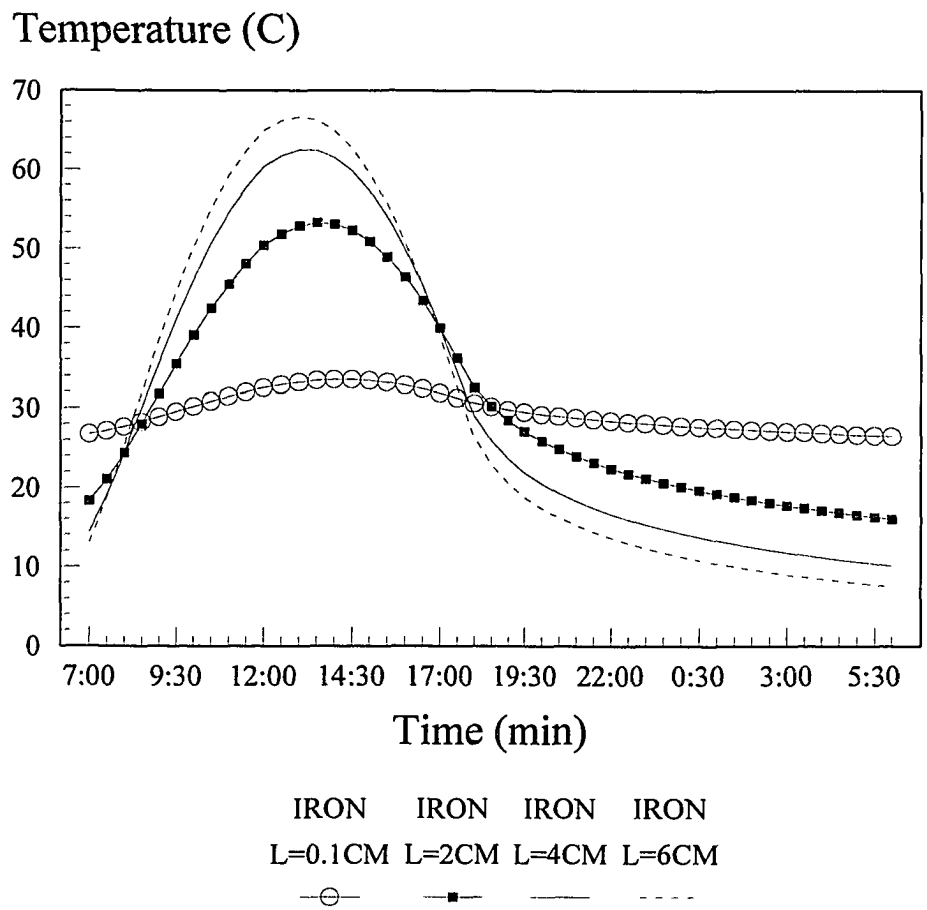


Figure 1-4
Mathematical model of diurnal solar radiation heating source with a metal object buried at different depths under sand.

diurnal changes produced by solar radiation can be seen and be used to identify buried objects. But it is a relatively slow effect, with measurable changes manifesting in hours. The best times to observe the temperature differences are pre-dawn and shortly after noon, since the temperature differences at these two times are greater than the other times.

### 2.2.3 Basic model for step function radiation

For a step function radiation heating source, the flux on the surface of the ground needs to be changed. Since we still need to consider the radiation from sky and from the ground in our indoors experiment, the only term need to change in the flux on the ground in (1.8) is $FS_n$, which will be the radiation flux from an artificial heating source, (a step function). We experimentally determined the flux value of our radiation source.

In the experiment, we used a power meter to measure the power of the surface of the ground after the radiation was switched on. As seen in Figure 1-5, we placed the power meter on the surface of our sand box. Four lamps were used as our step function heating source. Since the sensor of power meter was facing up, the reading from the power meter indicated the power absorbed by the surface only, i. e. in the equation (1.8), only first two terms' power were be taken. $FA_n$ could be calculated according to the room temperature (indoors). So the flux of step function radiation source will equal the flux from the measurement minus the flux due to sky's radiation. The average power we got was about 0.8 Watt for these four lamps radiation source, when the lamps are switched on. Combined with the radiation flux from sky, the flux of the radiation is 0.0365 Calories / Second / $cm^2$. When the lamps are switch off, no radiation comes from the artificial heating source, and the absorbed flux on the surface of the ground depends on the sky radiation, which is the effective room temperature.

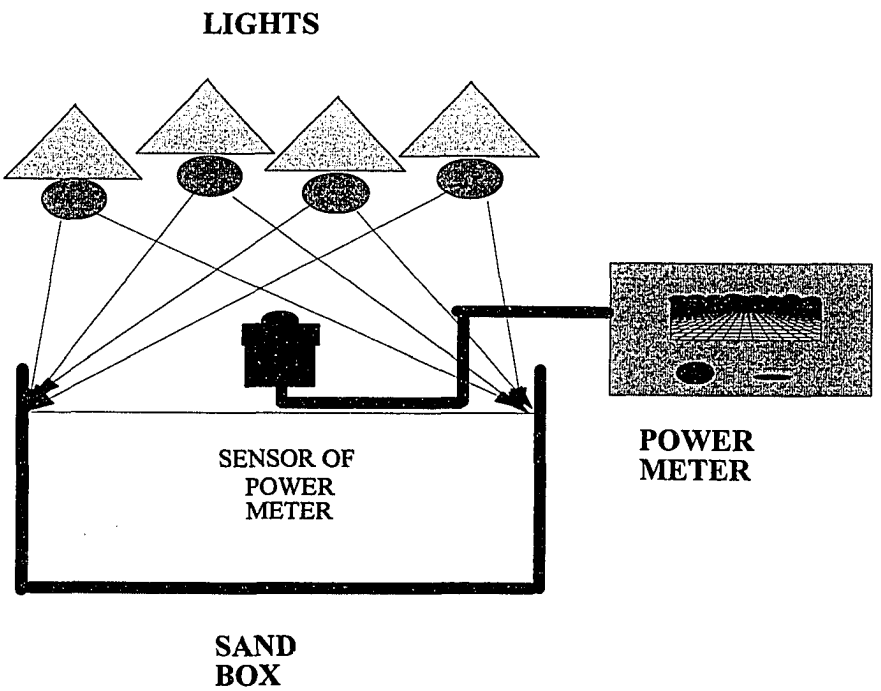


Figure 1-5
Experiment set-up for the measurement of flux of the radiation source.

In Figure 1-6 and Figure 1-7, plastic, metal and rock are buried under dry sand staggered at the same depth: 0.3 cm in Figure 1-6; and 1 cm in Figure 1-7. The heating time of step radiation is four hours. With step function radiation flux, the temperature is increased in all situations when the lamps are on. The surface temperature reaches its maximum temperature at the precise point that the lamps are switched off. Again, buried objects with lower thermal properties reach a higher temperature and their changing rate is higher than the objects with higher thermal properties. When radiation is removed, temperatures start to decrease at different rates depending on the thermal properties of various buried objects.

For plastic, which has a small thermal inertia and low heat conductivity, the heating and cooling rates are both relatively large. Thus, with a plastic object buried under sand the surface temperature increases during the lamps-on time and cools during the lamps-off time at a faster rate than the surface of the sand with no buried object. Consequently, the surface temperature over a plastic object is higher than that with no buried object during the lamps-on time and then switches to becoming lower than that of the surroundings as the lamp radiation is switched off and the soil cools.

For a metal, which has a large thermal inertia and heat conductivity, the heating and cooling rates are slow. So with a metal object buried under the sand, the surface temperature increases during the lamps-on time and decreases during the lamps-off time at a slower rate than that of the sand's surface with no buried object. As a consequence, the surface temperature over a metal object remains lower than sand's surface with no buried object during the lamps-on time and then switches to becoming higher during the lamps-off time.

The rates of temperature change depend on the depth of the sand layer over the buried object as well (see Figure 1-6); while the rate for plastic decreases with depth, the

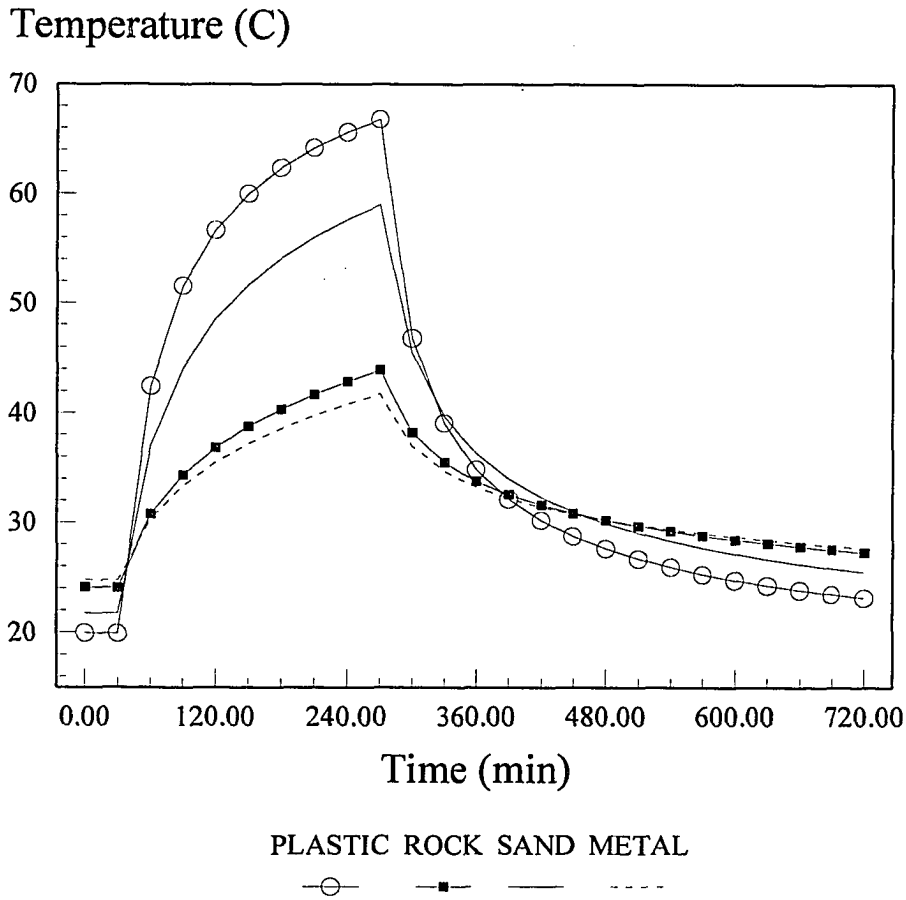


Figure 1-6
Mathematical model of step function heating source with plastic, rock and metal buried under sand, sand depth L = 0.3 cm.

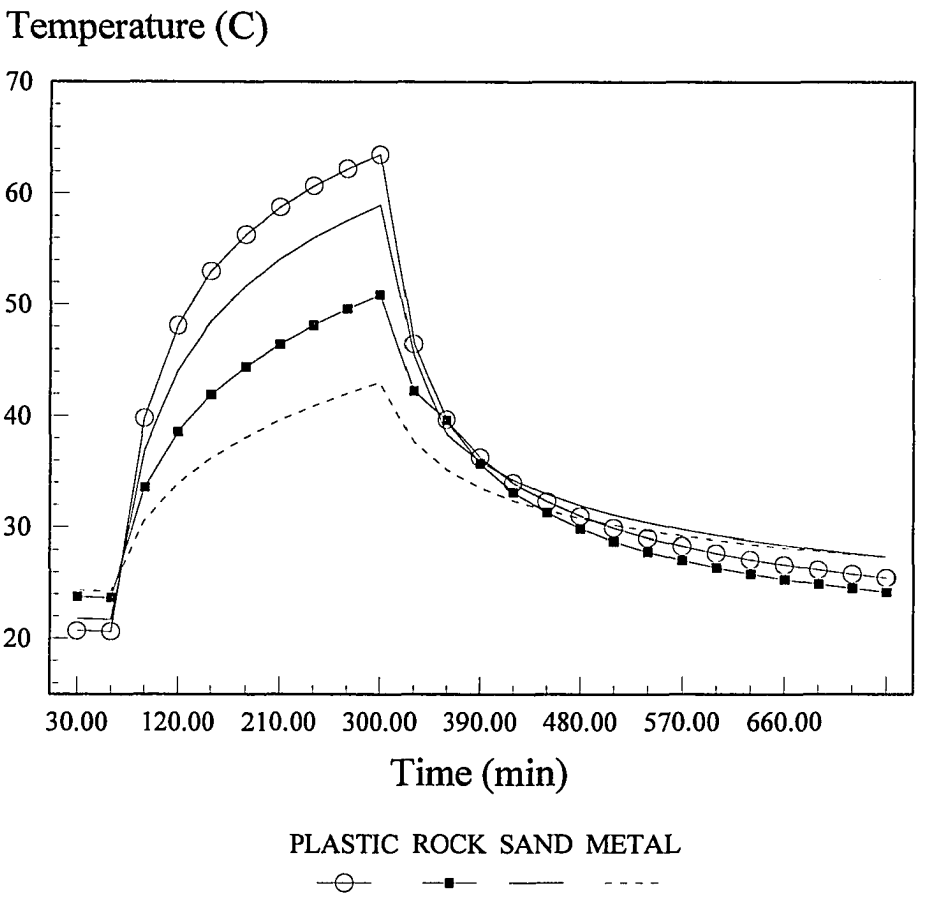


Figure 1-7
Mathematical model of step function heating source with plastic, rock and metal buried under sand, sand depth L = 1 cm.

rate for metal increases with depth. This effect is better outlined in Figure 1-7 where we plot the simulations for plastic buried under various depths of sand. As the depth of the layer of sand is increased, the surface temperature response converges to that of a semi-infinite sand layer.

$T_{dec}$ is defined to indicate the time interval when the surface temperature above a buried object reaches the same surface temperature as sand-only. After the time of $T_{dec}$, surface temperatures above a buried object will change in the opposite direction to sand-only surface temperatures. For example, with a buried plastic object, the surface temperature is higher than the sand-only surface temperature before $T_{dec}$, and lower after $T_{dec}$. An object with lower thermal properties has a smaller $T_{dec}$. For an object which has higher thermal properties (like metal), $T_{dec}$ becomes smaller as the buried distance increased. For an object which has lower thermal properties (like plastic), $T_{dec}$ becomes bigger as the buried distance increases. At the same time, the rate of decrease can be used to distinguish different objects. The decreasing rate, $R_{dec}$, is the ratio of surface temperature difference at the time radiation is switched off, minus the temperature at the observation time, $T_{obs}$, to the observation time $T_{obs}$. The increasing rate, $R_{inc}$, is the ratio of surface temperature difference to the temperature at the time radiation is switched on minus the temperature at the observation time, $T_{obs}$, to the observation time $T_{obs}$. Data in Table 1 are taken from Figure 1-6 and Figure 1-7. From Table 1, it can be seen that: 1) as distance increases, the increasing rate, $R_{inc}$, and decreasing rate, $R_{dec}$, move towards these of sand-only; 2) usually, the increasing rate is greater than the decreasing rate for each object. Figure 1-6 and Figure 1-7 shows at the onset of radiation, the surface temperature of all buried objects stays almost the same as the sand-only surface (temperature difference $< 0.1^{o}$ C). We call this interval non-distinguished time, $T_{no}$, which differs when the depth differs. When buried plastic distances equal 0.3 cm, and 1 cm, then $T_{no}$ equal 7 minutes, and 9 minutes respectively.

The simulations above are reasonable approximations to these of the temperature of sand above the center of a buried object so long as the depth of the sand layer above the object is much less than the object's dimensions. Even under this condition, there is still another short-coming of this model in that radial heat flow is not taken into account. However, in spite of these short-comings, as shown in the next section, the simulations are in good agreement with the experimental data in the surface temperature during the thermal excitations.

| Depth | L=0.3 cm | | | L=1 cm | | |
|---|---|---|---|---|---|---|
| Material | $T_{dec}$ min | Rdec (%) | Rinc (%) | Tdec min | Rdec (%) | Rinc (%) |
| Plastic | 50 | 12 | 17 | 60 | 10 | 16 |
| Avg. Rock | >200 | 4 | 6.8 | 110 | 5.6 | 11 |
| Aluminum | >200 | 2.6 | 6.3 | 190 | 2.6 | 7.8 |
| Dry Sand | .. | 7.9 | 14 | .. | 7.9 | 14 |

Table 1
*Decreasing time $T_{dec}$, decreasing rate $R_{dec}$ and increasing rate $R_{inc}$ of different objects at different depth.*

Figure 1-8 and Figure 1-9 showed the effects of heating time $T_h$. The buried object is plastic at respective depths of 0.1 cm and 1 cm. The heating times $T_h$ equal 4 hours in Figure 1-8 and 2 hours in Figure 1-9. The longer the heating time, the higher temperature can be reached and the faster the time it takes to decrease. At the depth of 0.1 cm the decreasing time is 50 minutes; 80 minutes when heating time equals 4 hours and 2 hours, respectively.

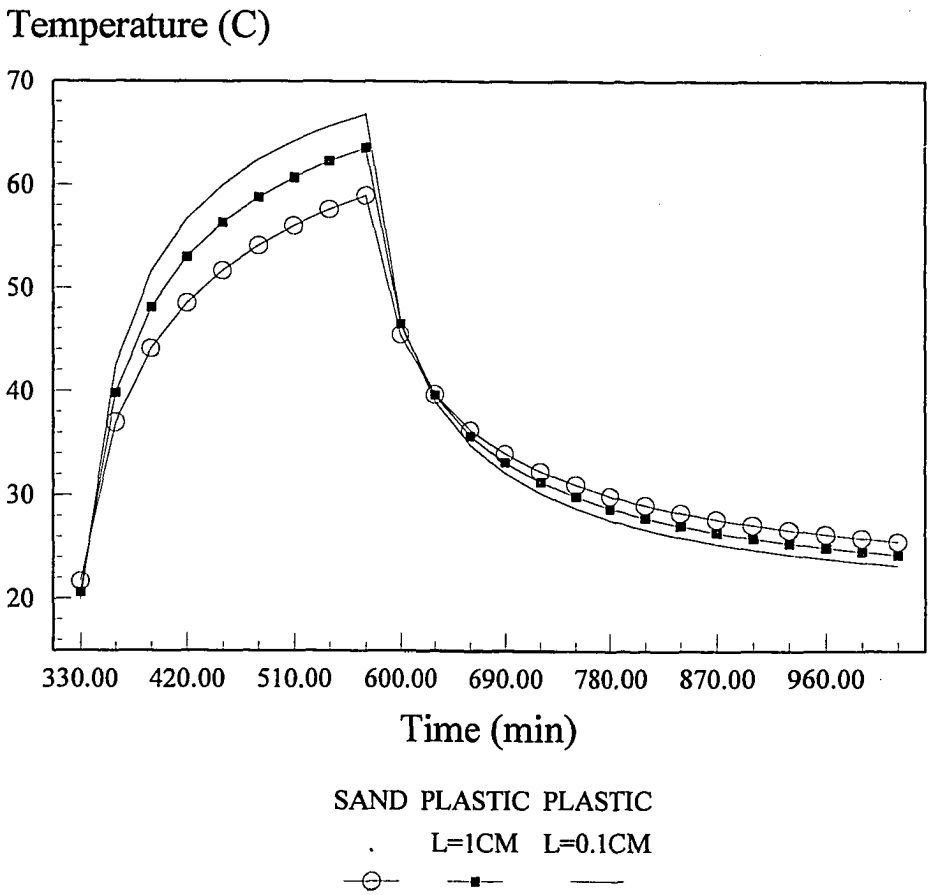


Figure 1-8
Mathematical model of step function heating source with a plastic object buried under sand at different depths. Heating time is 4 hours.

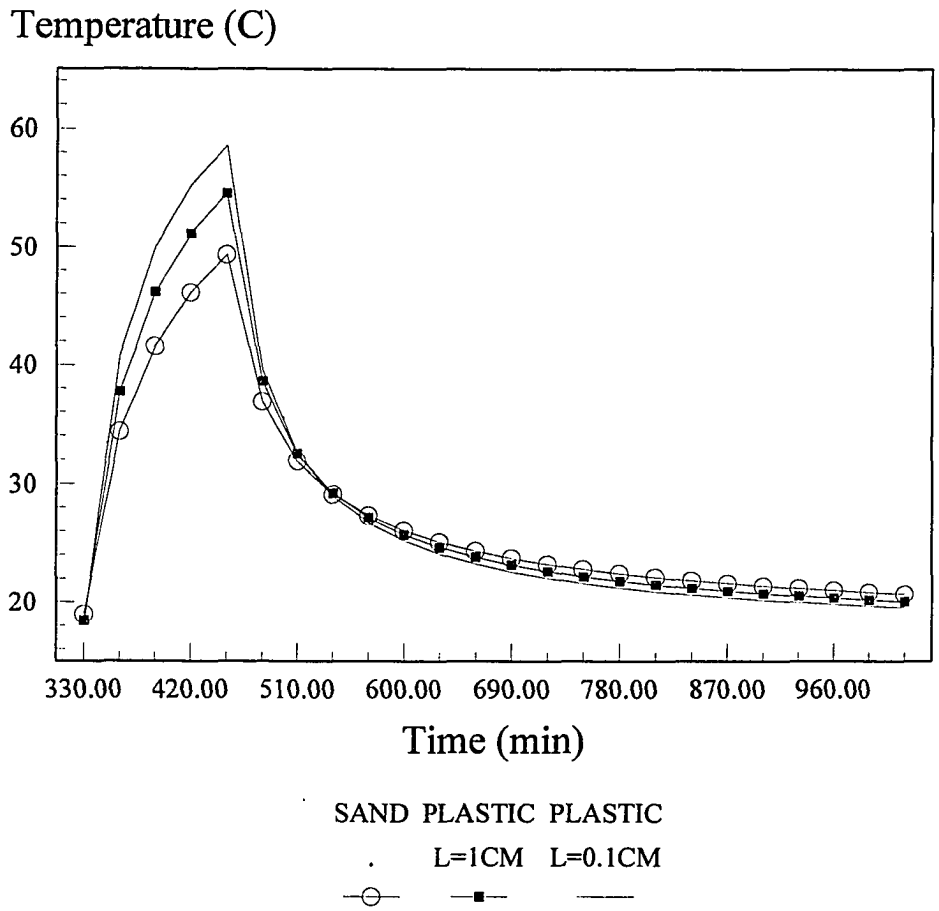


Figure 1-9
Mathematical model of step function heating source with a plastic object buried under sand at different depths. Heating time is 2 hours.

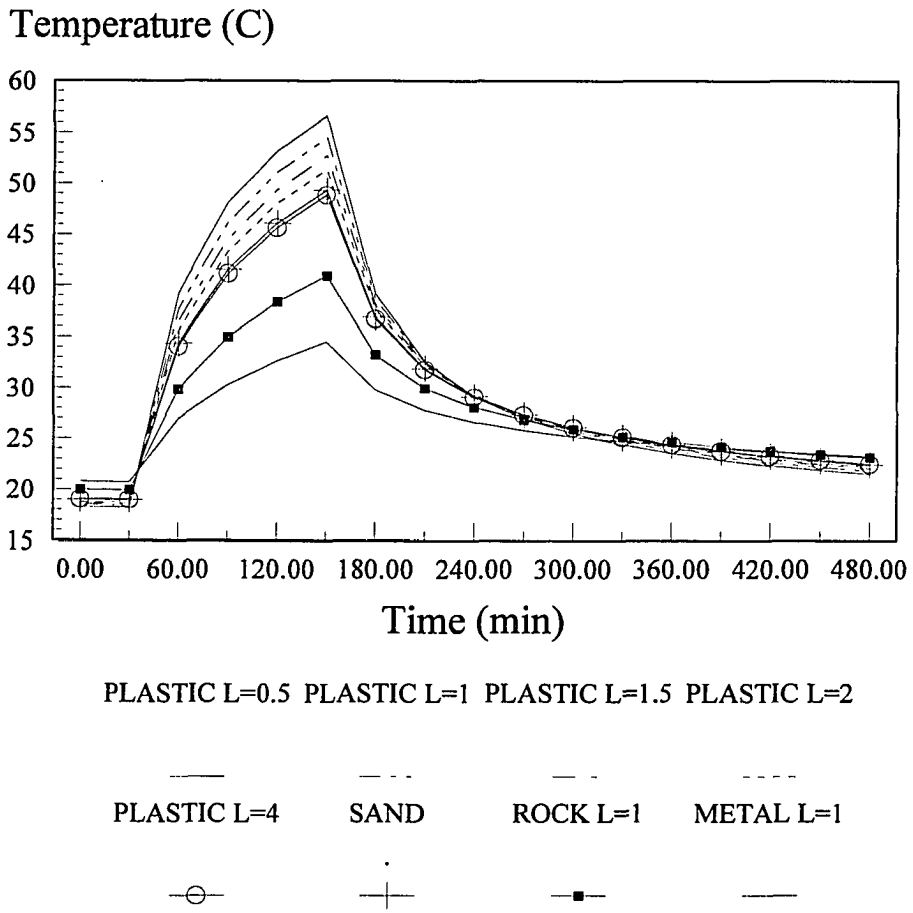


Figure 1-10
Surface temperature with a plastic object buried at different depths, a rock and a metal object buried at depth L = 1 cm, heated by a step function radiation source for four hours.

The difference of the same material objects at different depths and the different material buried at certain depths is presented in Figure 1-10. Figure 1-10 plots surface temperature when plastic objects are buried at distances of 0.5 cm 1 cm, 1.5 cm, 2 cm; a metal and an average rock each buried at a distance of 1 cm under dry sand. The heating time, $T_h$, for these varied materials is two hours. The results show during radiation on, a plastic object (which has lower thermal properties than sand) will cause the maximum surface temperature to be higher than the sand-only surface temperature; and its temperature increase rate is always greater than that of sand-only. The convergence point is the sand-only temperature increase rate. In the cooling process (radiation off), plastic at any buried distance will cool at a faster rate than sand-only. The temperature decrease rate of a plastic object moves towards that of sand as the distance increases. However for the metal and rock objects, since their thermal properties are higher than sand's, the temperature above them can never be higher than sand-only surface temperature when the radiation is on, and their rate of decrease will always be smaller than sand's when the radiation is off. So we can distinguish plastic from metal and rock by noting the temperature increasing and decreasing rates.

We conclude our results in Table 2.

With a step function heating source, all those factors like, maximum temperature $T_{max}$, decreasing time $T_{dec}$, non-distinguished time $T_{no}$, decreasing rate $R_{dec}$, and increasing rate $R_{inc}$, can be used to detect the possibly existing buried objects at their submerged depths as previously discussed. Since non-distinguished time, $T_{no}$, with step function heating source occurs within several minutes of the heating cycle, this method for real time detection is more practical. Choosing a different heating time, $T_h$, will affect the factors in the cooling process; the longer the heating time, the easier and quicker it is to detect a buried object. However the price paid is waiting through that long heating

time. Compared to a diurnal heating source, a step function heating source can get results in much less time.

| | COMPARED TO SAND | | BURIED DISTANCE INCREASED | |
|---|---|---|---|---|
| THERMAL PROPERTIES | Higher (Metal, Rock) | Lower (Plastic) | Higher (Metal, Rock) | Lower (Plastic) |
| Max.Temp. T | Lower | Higher | ↑ | ↓ |
| $T_{dec}$ and $T_{no}$ | Bigger | Smaller | ↓ | ↑ |
| $R_{dec}$ and $R_{inc}$ | Smaller | Bigger | ↑ | ↓ |

Table 2
*Maximum temperature T, decreasing time $T_{dec}$, non-distinguished time $T_{no}$, decreasing rate $R_{dec}$ and increasing rate $R_{inc}$ comparison*

These mathematical models basically express the behavior of temperature changes to the object buried under the ground with step function radiation.

## 2.3 Experiment works

### 2.3.1 The system description and experiment set-up

The system we have established will use an infrared camera to collect thermal infrared images, analyze and process the infrared images and their data, abstract as many

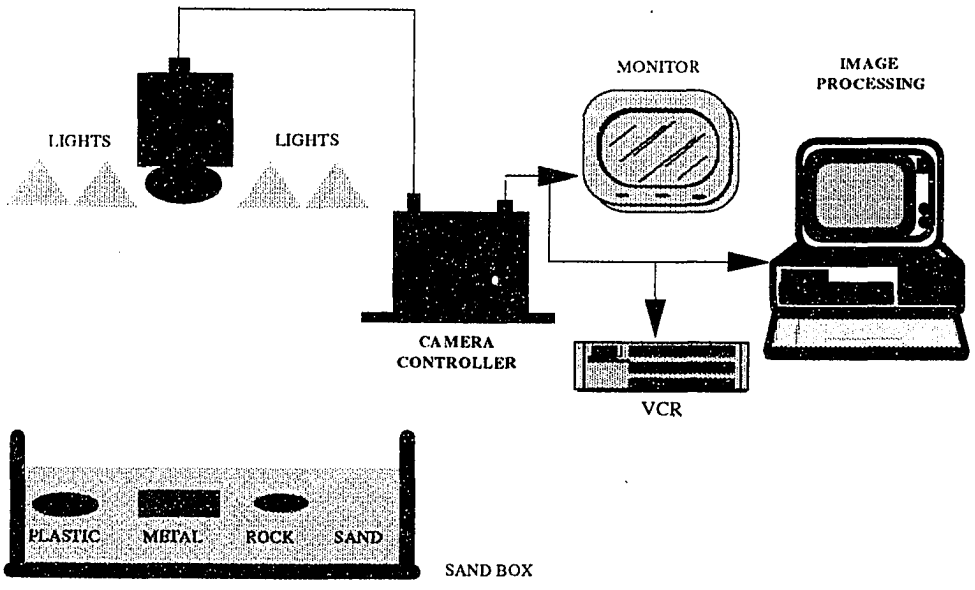


Figure 1-11
The Close In Detection of Buried Objects Using An Infrared Imaging System

features of temperature distribution on the surface of the soil under different circumstances as possible, and recognize possible buried objects automatically.

Our experiment is shown in Figure 1-11, which: 1) examined the theoretical model given in Section II; 2) studied the temperature changes on the surface of the sand with and without buried objects.

In our experiment, the camera (a "smart" Model 740 Thermal Infrared Imaging camera from Inframetrics, Inc) was mounted on a 5' platform that also houses four 250 Watt infrared heating lamps. At the base of the platform was a cardboard box ( 20" long, 17" wide and 13" deep) filled with sand and containing buried test objects (see Figure 4). The test site was exposed to a step function variable irradiation by four heat lamps. Resulting thermal changes were observed and recorded by the camera system as well as a VHS video recorder. The lamps were positioned to achieve the best illumination uniformity over the surface of the sand. A 14" Sony high resolution color monitor was also connected to the camera controller to increase the experimenter's ability to better observe the changes in the thermal image.

The digitally recorded images from the camera controller were further processed using a 486 DX2/66 MHz personal computer and the pseudo color temperature images were printed by a Hewlett Packard Model 1200 color printer.

### 2.3.2 Experiments and results discussion

#### 2.3.2.1 The surface temperature of different objects buried at same depth

In these experiments, there are several objects buried under the surface of the sand at a distance of 0.3 cm. The actual shapes of these objects are shown in Figure 1-12. The metal is a 0.75" thick piece of aluminum. The metal reference is a 0.25" thick aluminum piece placed on top of the sand. We used four infrared lamps as our step function heating radiation, turning them on and off. During experimental runs, digital recordings of

temperature images at various intervals ranging from 1 minute to several hours were carried out. A sample image is shown in Figure 1-13. Each gray level in this image corresponds to a different temperature as indicated by the gray chart at the bottom of the Figure 1-13. This image was taken during a heating phase using the heat lamps and shows that the surface of the sand over the plastic object reaches the highest temperature than the surface anywhere else in the test site. The color contours, which correspond to temperature contours are in the shape of the buried objects. Also notable are the slight variations of the surface temperature in the areas where there are no buried objects. This variation is most likely due to such factors as sand density packing and sand moisture.

In Figure 1-14, we plotted the summary of results from an entire heating and cooling cycle consisting of lamps time-on of 4 hours and lamps time-off of 4 hours. The sand surface temperatures over various object were recorded from points directly over the center of the objects. The sampling interval in this run was in 5 minute segments. These results are qualitatively consistent with the theoretical results plotted in Figure 1-6. The sand surface over the plastic object heats up at a faster rate than the others and cools at a faster rate than the others. It also reaches the hottest temperature relative to others during the heating cycle and the coolest temperature relative to others during the cooling cycle. The surface temperature over the metallic object behaved in just the opposite way: heating and cooling at the slowest rate and being the coolest surface during the heating cycle and the warmest surface during the cooling cycle. Temperature variations over the surface of the buried rock depended on the rock's composition. The temperature changes of the soil surface with no buried objects have intermediate heating and cooling rates as well as temperatures. This is consistent with our theoretical model and easily

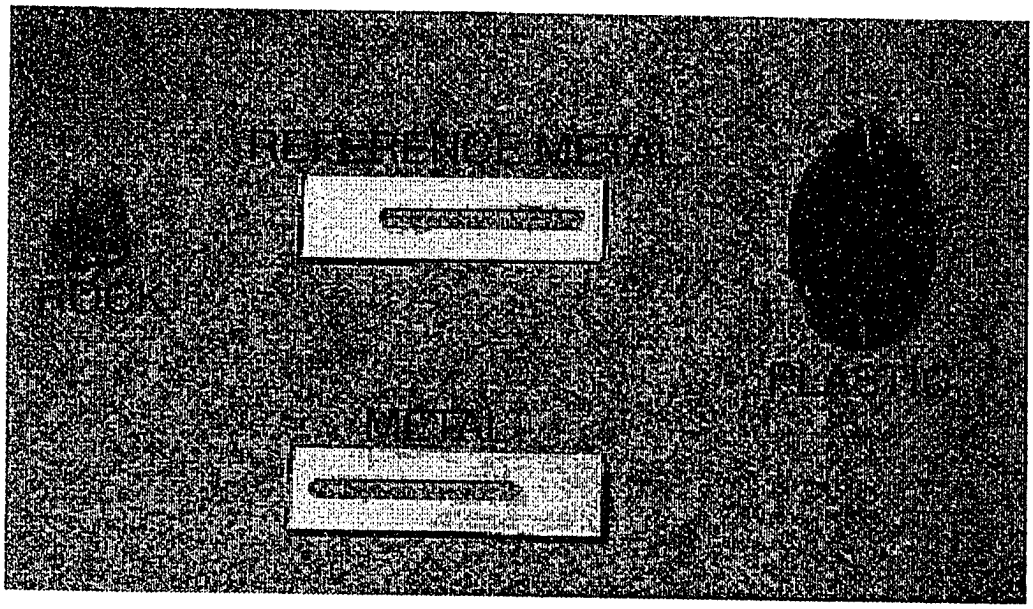

Figure 1-12
Objects and their positions in tests. Image taken before they are buried.

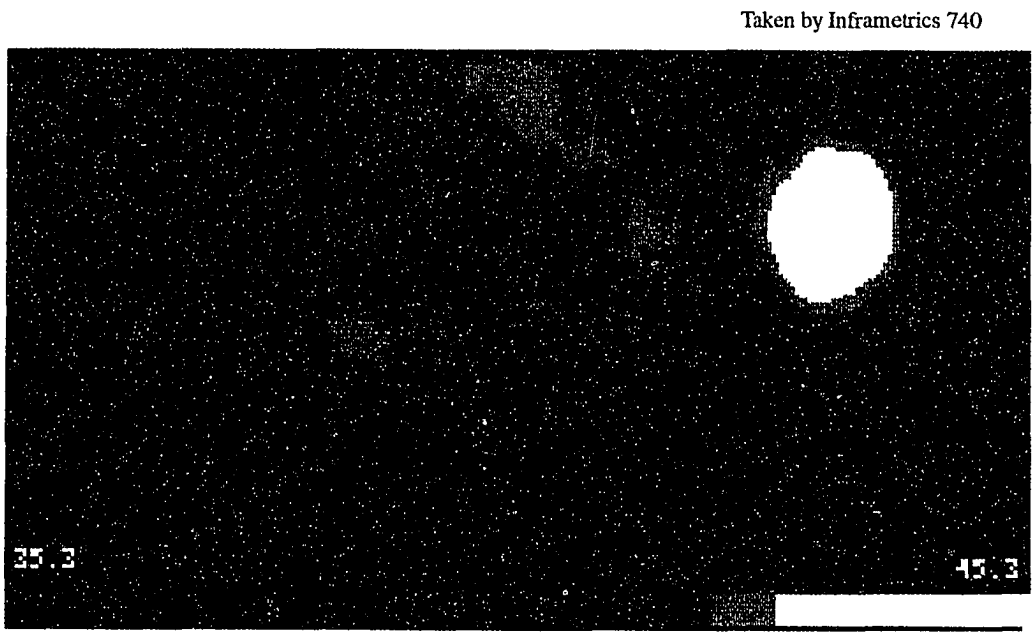


Figure 1-13
Infrared image of surface temperature taken by Inframetrics Model 740 camera after 10 minutes heating experiment on July 30, 1993.

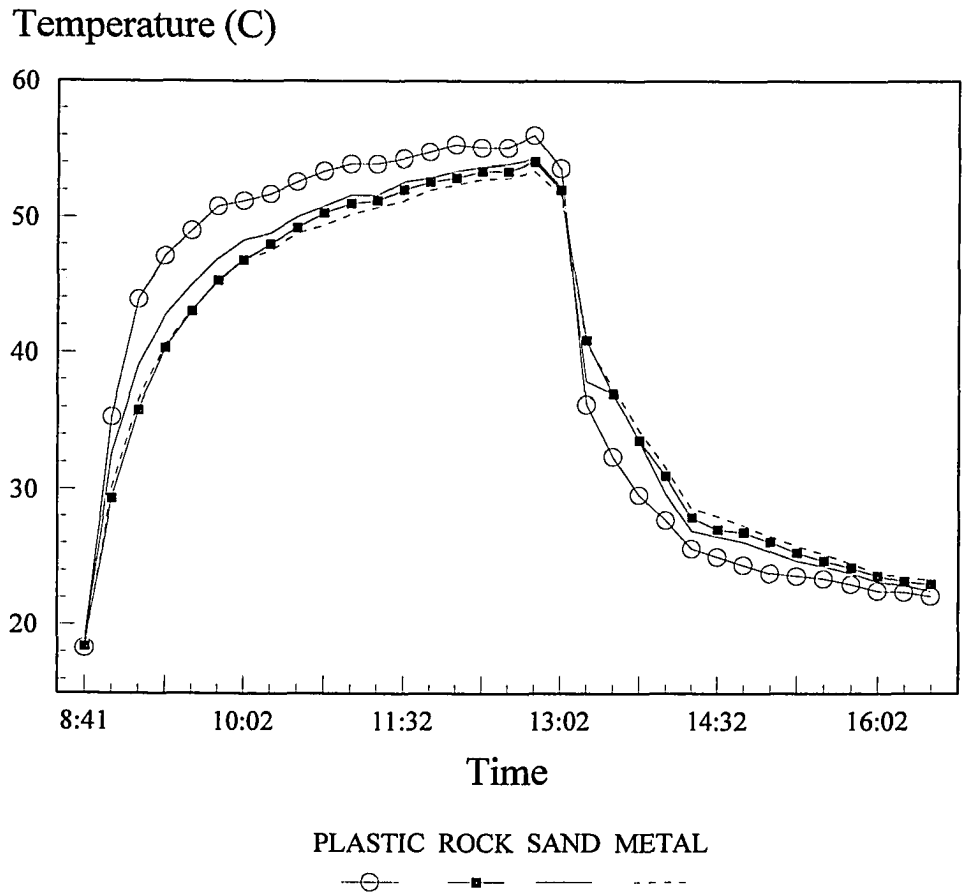


Figure 1-14
Surface temperature with plastic, rock and metal objects buried under sand. Data collected from experiment on July 30, 1993.

understandable due to plastic's low thermal conductivity and heat capacity versus the metal's large conductivity and heat capacity.

In both heating and cooling cycles at any time interval, the change of surface temperatures over the plastic objects is higher than over all the other objects. It is notable that for all the cases with or without objects buried in the ground during the heating cycle, the surface temperature changes faster than in the cooling cycle at any observing time. This actual result is the same as our theoretical result. In the first 10 minutes of either heating or cooling cycles the surface temperature changes faster than any time thereafter. During the cooling process, this actual time of change was shorter than results from theoretical calculation primarily because the starting temperature in the actual experiment was lower than the theoretic calculation, and in the theoretical calculation we assumed the step heating source was a periodic signal.

Next, we studied the rates of cooling and heating of the surface over various objects at closer time intervals and under similar experimental conditions. Again, the figures clearly show the largest rate of change for the plastic object. As we found before, plastic's rate is higher in any time interval. However it is clear that the changing rate of the first 10 minute's is much larger than that of 1 hour and 4 hours for both cooling and heating cycles. As the time increases, the rate of change decreases.

2.3.2.2 The surface temperature of plastic object buried at different depths

Figure 1-15 shows the results of an experiment wherein round plastic objects (4 1/2" in diameter and 2 1/2" thick), buried at distances of 0.5 cm, 1.0 cm 1.5 cm and 2 cm, heated using a step function heating source for 2 hours, then cooled for another 2 hours. The images of the first hours (when lights were either on or off) were taken at 2 minute

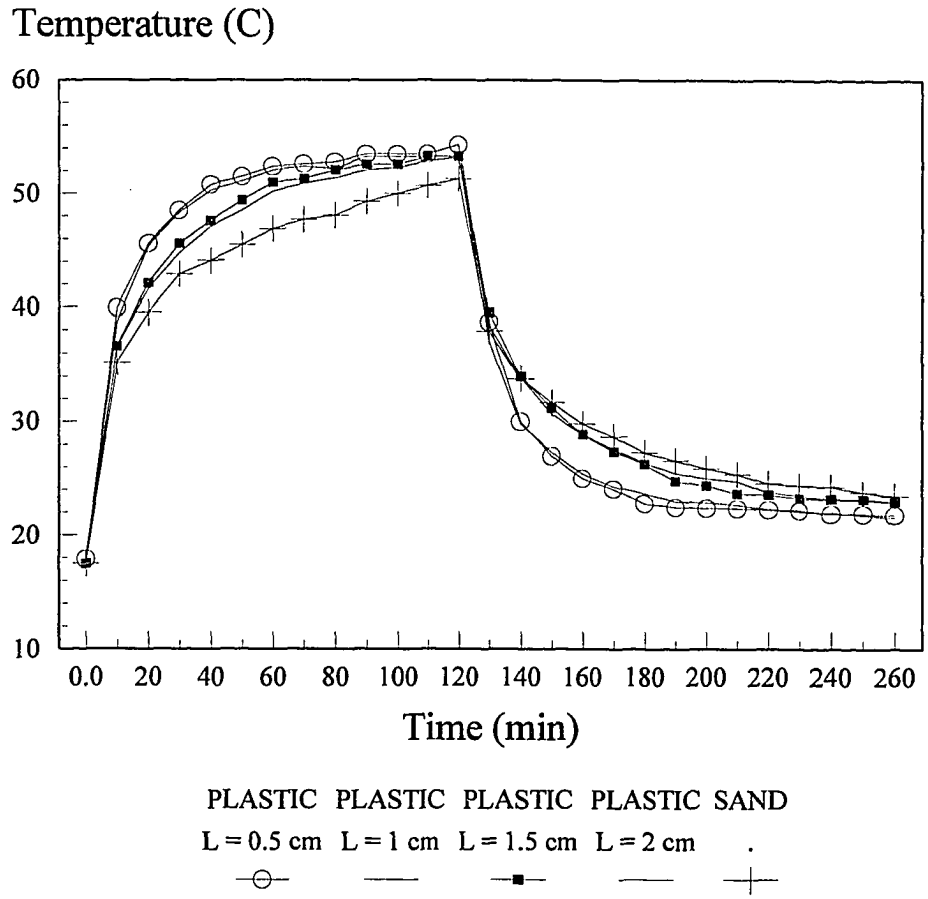


Figure 1-15
Experiment results of step function heating source with plastic buried under sand at different buried depths (L = 0.5 cm, 1 cm, 1.5 cm and 2 cm). Heating time is 2 hours.

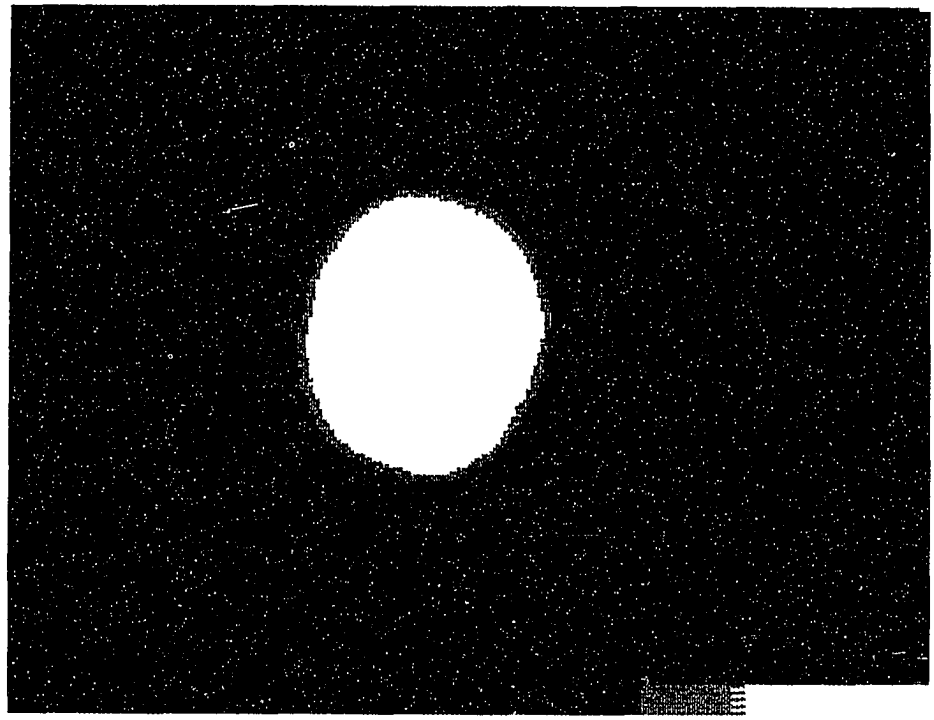

Figure 1-16
The infrared image of surface temperature of sand with a plastic object buried at 0.5 cm, after 30 minutes heating. Experiment on May 28, 1994.

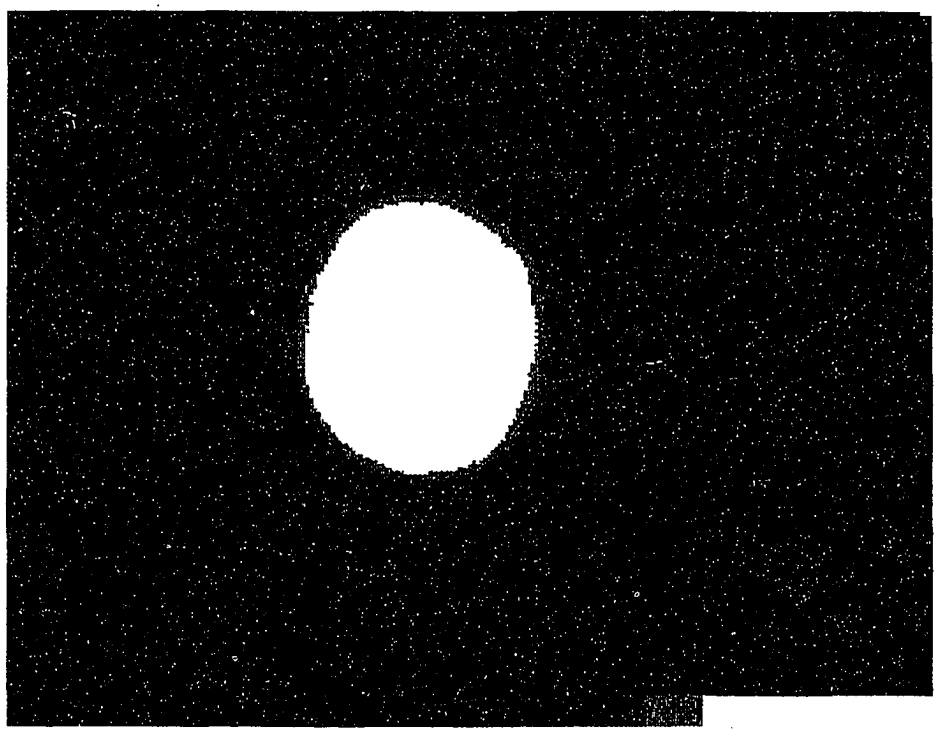

Figure 1-17
The infrared image of surface temperature of sand with a plastic object buried at 1 cm, after 30 minutes heating. Experiment on May 29, 1994.

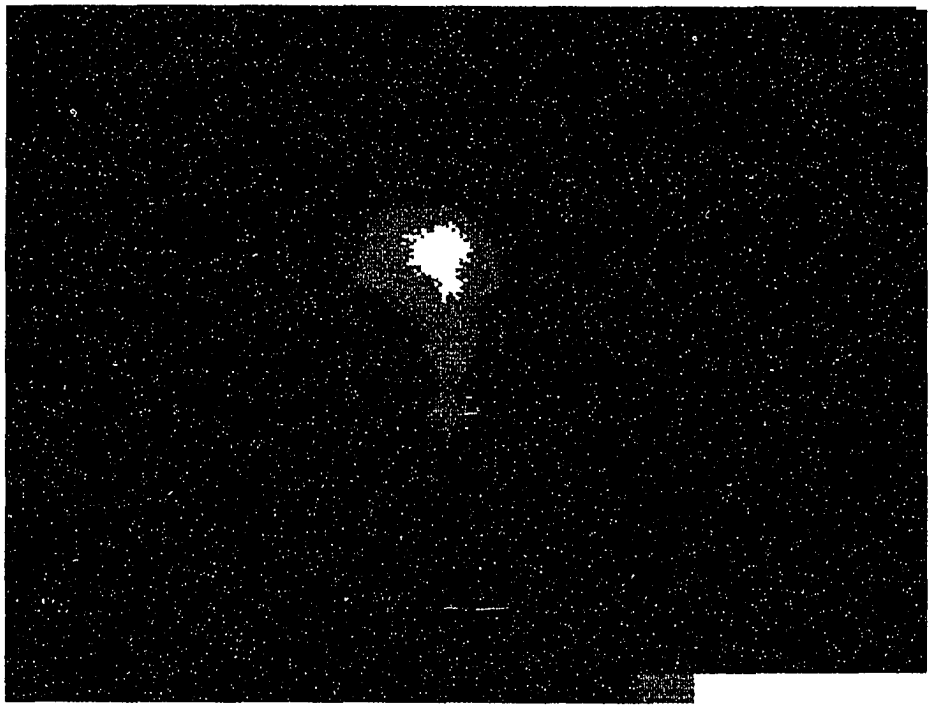

Figure 1-18
The infrared image of surface temperature of sand with a plastic object buried at 1.5 cm, after 30 minutes heating. Experiment on May 30, 1994.

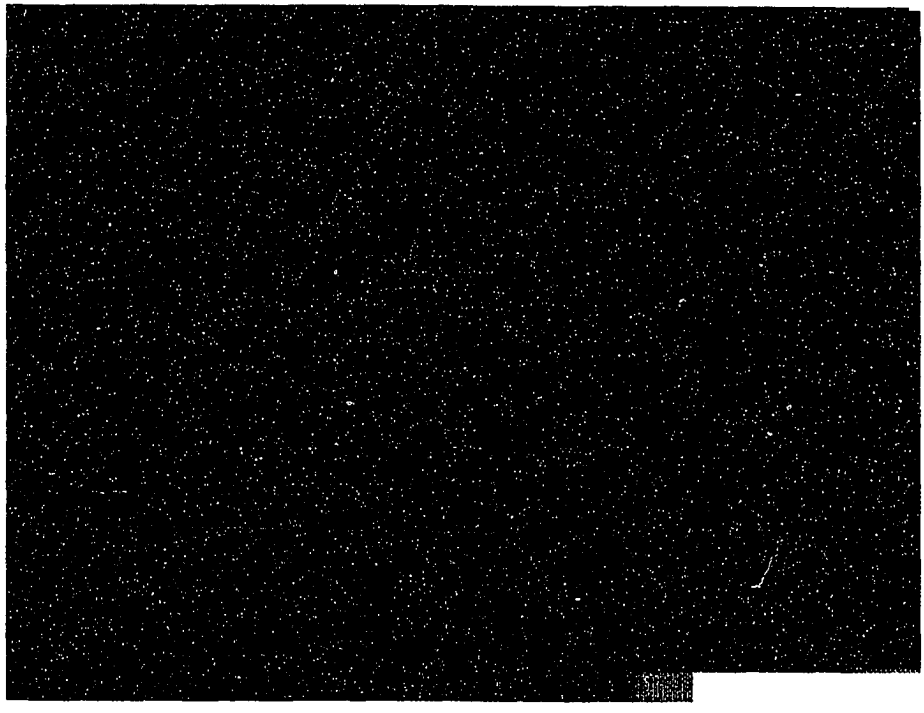

Figure 1-19
The infrared image of surface temperature of sand with a plastic object buried at 2 cm, after 30 minutes heatin. Experiment on May 31, 1994.

intervals and the images of the remaining time were taken at 10 minute intervals, which were done on May 28, 29, 30 and 31, 1994, individually.

Figures 1-16, 1-17, 1-18 and 1-19, are sample infrared images of a plastic object buried at 0.5 cm, 1 cm, 1.5 cm and 2 cm. All four of these images were taken after 30 minutes lights-on and the temperature range was the same; that is, between 38.9° C to 48.9° C. Comparing these images, it is clear to see that as the buried depth became shallower ( as in Figure 1-16 ), the shape of the object could be seen more clearly; the surface above the object reached a higher temperature( as in Figure 1-19 ).

Table 3 is the data from the experiment performed on September 9, 1993. In the

| | COOLING | | | | HEATING | | | | | |
|---|---|---|---|---|---|---|---|---|---|---|
| PLASTIC | $T_{dec}$ min. | $T_{mx}$ (c) | $T_{30c}$ (c) | $R_{dec}$ c/mn | $T_{no}$ min | $T_o$ (c) | $T_{30h}$ (c) | $R_{in3}$ c/mn | $T_{60h}$ (c) | $R_{in6}$ c/mn |
| (L=0.5) | 12 | 55.7 | 25.8 | 0.99 | <2 | 15 | 48.9 | 1.13 | 52.1 | 0.62 |
| (L=1) | 18 | 53.9 | 27.4 | 0.88 | 3 | 15 | 46.2 | 1.03 | 50.6 | 0.59 |
| SAND | .. | 49.5 | 28.3 | 0.71 | .. | 15 | 41 | 0.87 | 46.2 | 0.52 |

Table 3
*Temperatures and the change rate.*
*Experiment performed on September 9, 1993.*

cooling cycle, $T_{dec}$ stands for the decreasing time interval when the surface temperature above a buried object reaches the same temperature as the sand-only surface. $T_{max}$ is the maximum surface temperature immediately before the heating source was removed. $T_{30c}$ is the observing time 30 minutes after the heating source was removed and $R_{dec}$ is the rate of temperature change in that 30 minutes.

In the heating cycle, $T_o$ is the initial temperature, $T_{30h}$ and $T_{60h}$ is the temperature after the heat source was turned on for about 30 minutes and 60 minutes respectively, and $R_{inc3}$ and $R_{inc6}$ are the temperature change rates in 30 and 60 minutes. $T_{no}$ is non-distinguished time.

2.3.2.3 The surface temperature changes and the rate of changes driven by diurnal solar radiation

Using Infomatric infrared camera we also performed an outside experiment in August 4, 1993 which was a hot and cloudy day with a maximum temperature at noon about $38^{o}$ C. The sample we used is the same plastic same as we used in the experiment in Group One and we buried the it at 1 cm in dry sand in the box. The box was put outside the night before. We begain at 10:00 am and ended at 21:00. At about 17:00 the shadow of the building block the sun shine and the actual sun-set that day was about 19:30. Figure 1-16 gives the results of the experiment. It can be seen that before the sun was blocked the surface temperature above the plastic of object was higher than sand-only surface temperature. Sometimes when clouds sppeared, the temperature of the surface decreased. The area with plastic buried showed a temperature change faster than the other area. After sun-shine was blocked, the surface temperature changes smoothly. About an hour after sun-shine was blocked, the surface temperature with a plastic buried under sand became cooler than the others. The maximum surface temperature appeared between 12:30 and 14:00. Because a heavy little cloud moved back and forth, it was hard to tell exactly what time the maximum temperature occured. This experiment verifies the mathematical model we did before.

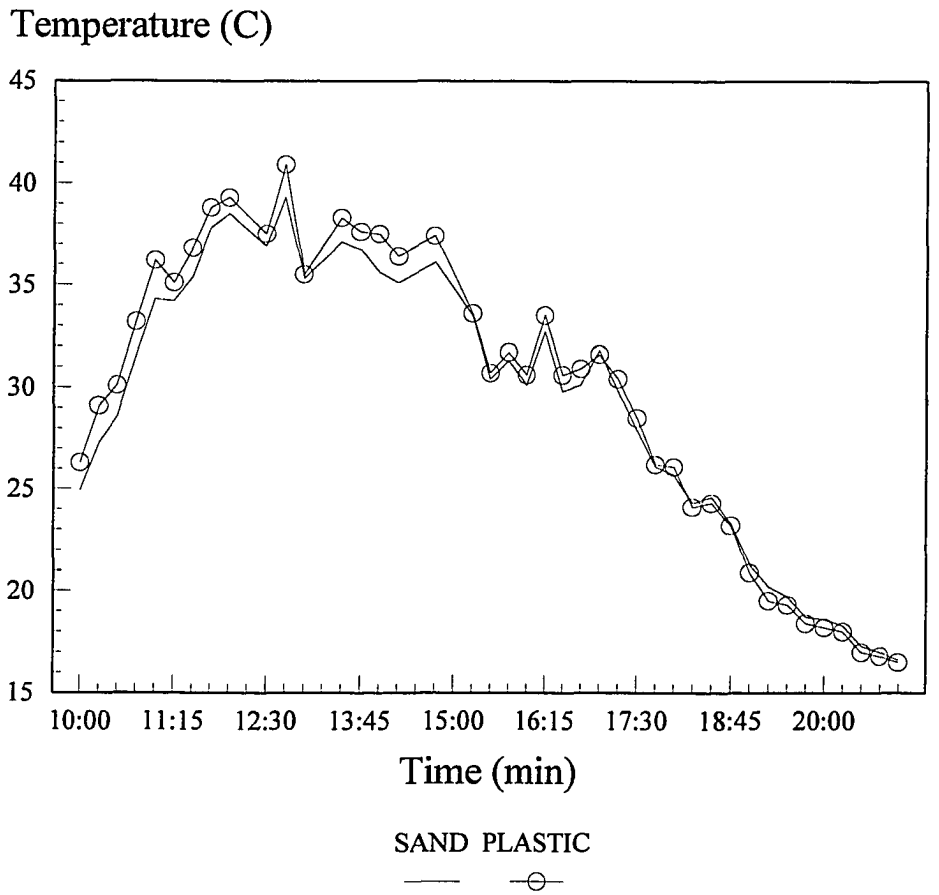


Figure 1-20
Experiment results of diurnal solar heating source with plastic buried under sand. Data collected from experiment on August 4, 1993.

## 2.4 Summary

The factors which distinguish the thermal imprints of the hidden objects from each other and from the surrounding sand are: maximum temperature, $T_{max}$, minimum temperature, $T_{min}$, the time when the maximum temperature appeared, decreasing time, $T_{dec}$, non-distinguished time, $T_{no}$, decreasing rate, $R_{dec}$ and increasing rate, $R_{inc}$. We can now systematically enumerate those factors for two methods of heating and cooling conditions: diurnal (natural) and step function (artificial).

### 2.4.1 Diurnal heating and cooling

In the diurnal heating and cooling process, the factors for detection are maximum temperature $T_{max}$, the time when the maximum temperature appeared, minimum temperature $T_{min}$, decreasing rate $R_{dec}$ and increasing rate $R_{inc}$ .

The rate of natural heating of the surface above buried objects of plastic, metal, rock or the surrounding sand, over a given time interval $T_{inc}$ are represented by the slopes of the lines A1P, A2M, A3S and A4R (see Figure 4-1). As detailed in previous Sections, the increasing slopes reflect the decreasing thermal inertia of the surface temperatures over a buried object during finite time intervals, and displays a series of different color-coded magnitudes which result in contours above the various buried objects. These temperature differences, combined with temperature difference contour geometry, assisted in buried object identification. Similarly, during the cooling cycle, different rates of cooling, as represented by the slopes B1P, B2M, B3R and B4S, were related to the different buried objects. The largest negative slope being related again to the material with the lowest thermal inertia (i.e. the plastic). Once again, the differences

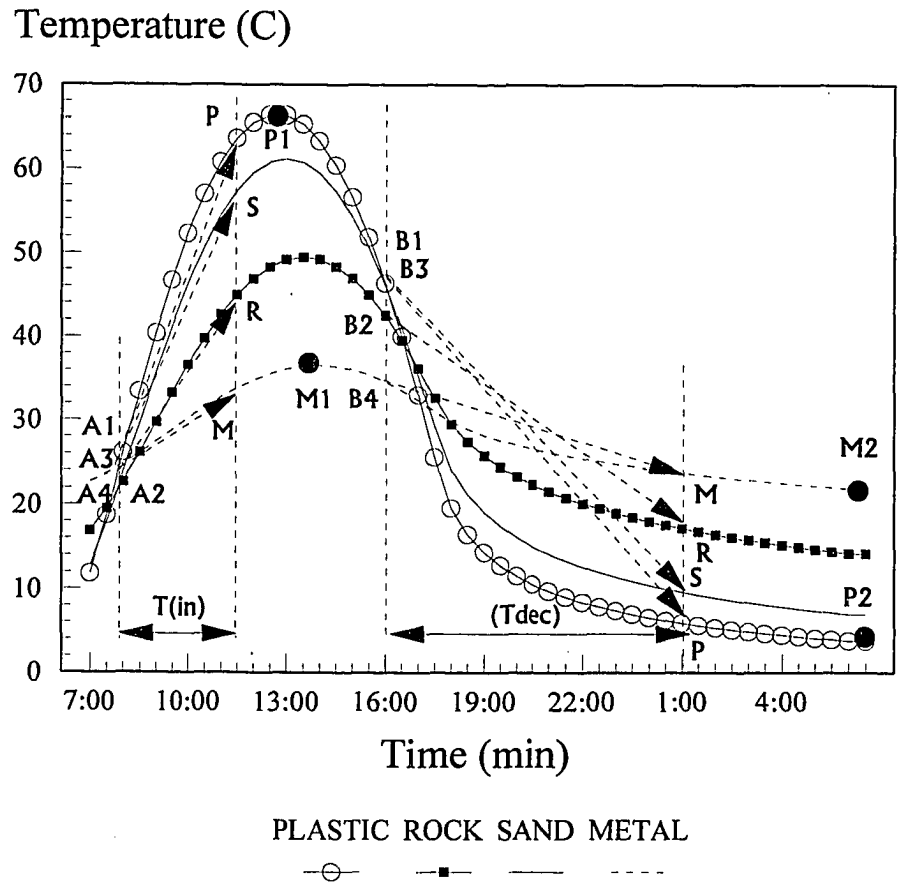


Figure 1-21
Mathematical model of diurnal solar radiation heating source with plastic, rock and metal buried under sand L = 0.3 cm, showing the maximum temperature and the rate of temperature change.

in the temperature changes over the finite time interval resulted in contours above the buried objects. This were used for their identification which was validated by both our theory and experiments.

The maximum temperature, $T_{max}$, becomes apparent on reviewing the entire heating-cooling cycle. For instance, the largest difference between the hottest observed surface temperatures and coldest, (points P1 and P2, in Figure 1-17), will be those related to surfaces above the plastic material, and the smallest differences will be those temperatures above the metal (between points M1 and M2).

The maximum temperature can be obtained shortly after noon. However this factor is heavily dependent on the weather conditions.

### 2.4.2 Step function heating and cooling

Artificial step function radiation can cause the surface temperature to change according to different objects buried under the soil. Using thermal infrared imaging techniques, the buried objects can be detected and the composition of the objects and their depths can be determined.

The factors which distinguish the thermal imprints of the hidden objects from each other and from the surrounding sand are: maximum temperature, $T_{max}$, minimum temperature, $T_{min}$, the time when the maximum temperature appeared, decreasing time, $T_{dec}$, non-distinguished time, $T_{no}$, decreasing rate, $R_{dec}$ and increasing rate, $R_{inc}$.

With a step function heating source, all those factors were used to detect the possible existence of buried objects and determine their buried depth as discussed previously. As non-distinguished time, $T_{no}$, in step function heating source occurs within several minutes of the onset of the heating cycle, the use of step function heating for real-time detection is more practical than using diurnal processes. Choosing a different heating time, $T_h$, will affect the factors in the cooling procedure: the longer the heating

process is, the easier and quicker the object is to detect; however the price paid is waiting for long heating time. Experimental results for step function heating and cooling strongly support their theoretic results. The changes in decreasing time, $T_{dec}$, and non-distinguished time, $T_{no}$, are mainly dependent on the depth of buried objects.

Step function heating or cooling of the sand enhances surface temperature differences over buried objects giving thermal infrared detection and identification a higher accuracy. In practice, for the above system and experimental conditions, buried objects can be differentiated in a time interval of the order of a minute either during cooling or heating. Besides the temperature resolution ($0.1^{o}$ C), this differentiation time depends on such parameters as the depth of the layer of sand, irradiation flux, and the size and the composition of the object.

As discussed earlier, the isotherm patterns in the sand above the buried objects would reflect their shapes. Additionally, the deeper the objects are buried, the isotherm patterns are more diffuse. Thus, analysis of the temperature gradients will yield an object's depth.

It was also observed that further detection enhancement is possible by subtracting an image during the heating cycle from that during the cooling cycle. We will discus this more in Part Two.

From the above discussion and observations, it is clear that along with conventional analysis of the geometric temperature distribution at a particular point during heating or cooling (via diurnal solar or artificial irradiation), incorporation of the surface rate of temperature change information into a detection scheme can significantly enhance thermal infrared detection capabilities.

## 2.5 References

[1] Richard D. Hudson, Jacqueline W. Hudson, "The Military Applications of Remote Sensing by Infrared", Proceedings of the IEEE, Vol. 63, pp.105-127, January, 1975.

[2] J. C. Jaeger, "Conduction of Heat in a Solid with Periodic Boundary Conditions, with Application to the Surface Temperature of the Moon", Proceeding Cambridge Phil. Society, 49 (2),355-359, 1953.

[3] Anne B. Kahle, "A Simple Thermal Model of the Earth's Surface for Geologic Mapping by Remote Sensing", Journal of Geophysical Research, Vol. 82, No.11, pp.1673-1680, April, 1977.

[4] Robert D. Watson, Brief Reports: "Surface-Coating Effects in Remote Sensing Measurements", Journal of Geophysical Research, Vol.75, No. 2, pp.480-484, January, 1970.

[5] Wiely D. H. Van Groningen, G. F. Vermeij, "Geometric Reconstruction of Buried Heat Sources from a Surface Thermogram", IEEE Transactions on Pattern Analysis and Machine Intelligence, Vol. PAM-7, NO. 5, pp.610-616, September 1985.

[6] Ingersoll, "Heat Conduction With Engineering", 1954.

[7] P. Concus, D. Caseate, G. Jaehning, "Tables for the Evaluation of $\int x^{\beta} e^{-x}(x)dx$ by Gauss-Lager Quadrature", Math. Computation, 17 (83), pp. 245-250, 1963.

[8] Kenneth Watson, L.P. Roan, T.V. Affiliate, "Application of Thermal Modeling in the Geologic Interpretation of IR Images", International Symposium on Remote Sensing of Environment Proceedings 8th, V.2. pp.1237, 1972.

[9] Kenneth Watson, L.P. Roan, T.V. Affiliate, "Application of Thermal Modeling in the Geologic Interpretation of IR Images", International Symposium on Remote Sensing of Environment Proceedings 7th, V.3 pp.2017-2041, 1971.

[10] Kenneth Watson, "Periodic Heating of a Layer over a Semi-Infinite Solid", Journal of Geophysical Research Vol. 78, No. 26, pp.5904-5910, September 1973.

[11] Charles Alice, "Introduction to the Physics and Techniques of Remote Sensing", Wiley Series in Remote Sensing.

[12] H. S. Carslaw, J. C. Jagger, "Conduction of Heat in Solids", Second edition, Oxford at the Clarendon Press.

[13] Kenneth Watson, "Geologic Applications of Thermal Infrared Images", proceedings of the IEEE, Vol. 63, pp.128-136, January, 1975.

[14] A. H. Stroud, D. H Secrest, " Gaussian Quadrature Formulas", Prentice - Hall, Englewood Cliffs, NJ, 1966.

[15] F. B. Hidebrand, "Introduction to Numerical Analysis", McGraw-Hill, New York, 1956.

[16] V. I. Krylov, "Approximate Calculation of Integral", MacMillan, New York, 1962.

[17] Lau, S. K., Almond, D. P., and Patel, P. M., "A Qauntitative Analysis of Pulsed video Thermograghic imaging of subsurface defects", in Photoacoustic and Photothermal Phenomena II, Springer Series in Optical Sciences, Vol 69, pp522-524 (Springer-Verlag 1992).

[18] Favro, L. D., Jin H. J., Kuo P. K., Thomas, R. L. and Wang, Y. X. "Real Time Thermal Wave Tomography", in Photoacoustic and Photothermal Phenomena II, Springer Series in Optical Sciences, Vol 69, pp519-521 (Springer-Verlag 1992).

# III. PART TWO

# Part Two

## 3.1 Background and problem

Based on the results of experiments we did in Part One we conducted some further works in Part Two. First, we modified our mathematical model for a finite-size buried object heating with step function radiation. Second, we studied the temperature distribution on the surface with a finite object buried. Last, we processed the data from the experimental thermal images.

Comparing Figure 1-6 with Figure 1-14 and Figure 1-9 with Figure 1-15, in Part One, several differences can be seen:

1) In experiments, after radiation removed several hours, the surface temperature will finally became uniform over the entire sand surface. This was the initial condition before each experiment. However theoretical results show that the surface temperatre dose not reach the same value over the buried objects, no matter how much the ratio of the cooling to the heating time interval of the periodic source function is increased.

2) The maximum theoretic temperature results were much higher than experimental results in all cases. And the first hour's temperature changing rate was much smaller than the experimental results.

The differences is due to the fact that, our theoretical calculations did not contain any radial heat flow term (as they are calculated for a semi-finite buried object). It is this heat conduction between the objects and their surroundings, that make the surface temperature become uniform if the flux on the surface dose not change for a relatively long time. So, it is necessary to modify our mathematical model, by considering these factors.

As we discussed in Part One, further detection enhancement is possible by processing data and image. Along with conventional analysis of the geometric

temperature distribution at a particular point during heating or cooling (via diurnal solar or artificial irradiation), incorporation of the surface rate of temperature change information into a detection scheme can significantly enhance thermal infrared detection capabilities. So in Part Two, we discussed more about further image and data processing.

## 3.2 Modification of mathematical model

Based on the previous discussion, a term related to the buried objects should also be included in the flux on the surface of the ground. This term will stand for the heat conduction between the finite object and the surroundings, as seen in Figure 1-1, the flux on the sides of the object. Then the flux on the surface will be:

$$F_n = F S_n + F A_n - F G_n - F B_n \tag{2.1}$$

here $FB_n$ is flux related to the finite size object. It is a function of the thermal properties, the size and the buried distance of the object. $FB_n$ will not only be included when the radiation is on, but also when the radiation is off, since after the radiation is off the flux on the sides of buried objects still exist. Based on the experimental results the approximately value of the sides' flux of $FB_n$ can be obtained.

The results showed in Figure 2-1 and Figure 2-2 were the calculated results from the mathematical model after modification. We used the same parameters as our

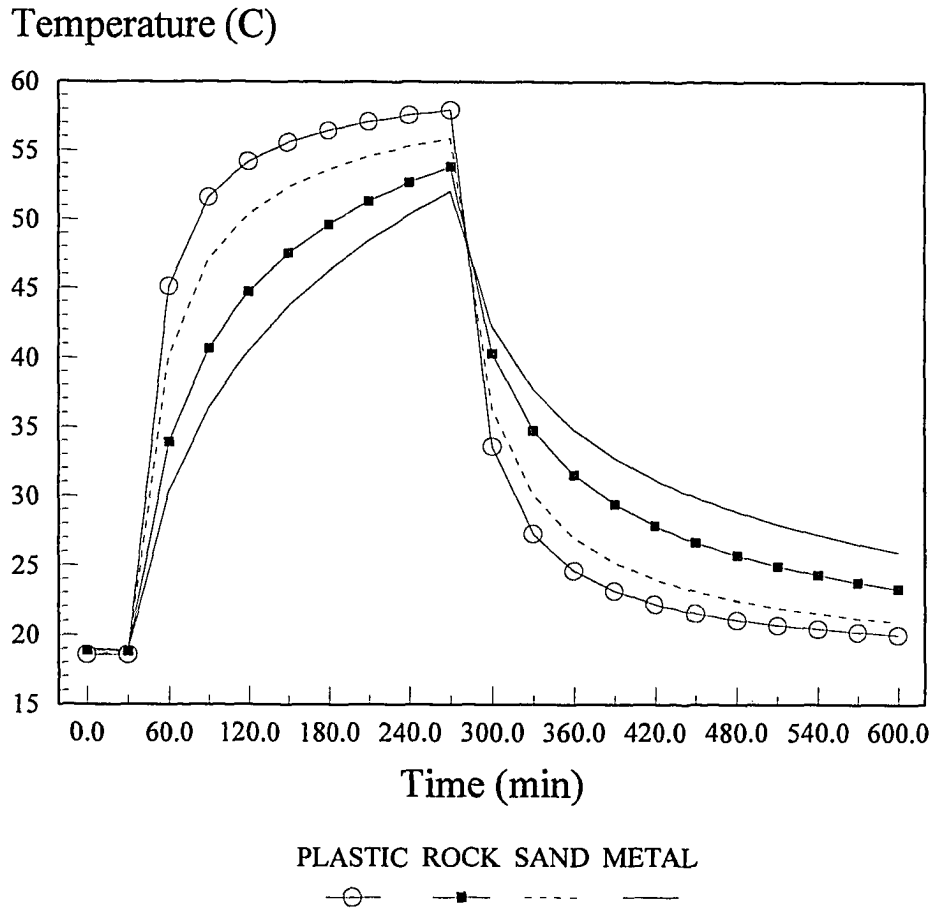


Figure 2-1
Modified mathematical model of step function heating source with finite size plastic, rock and metalobject buried under sand. The buried depth is L = 0.3 cm. The heating time is 4 hours.

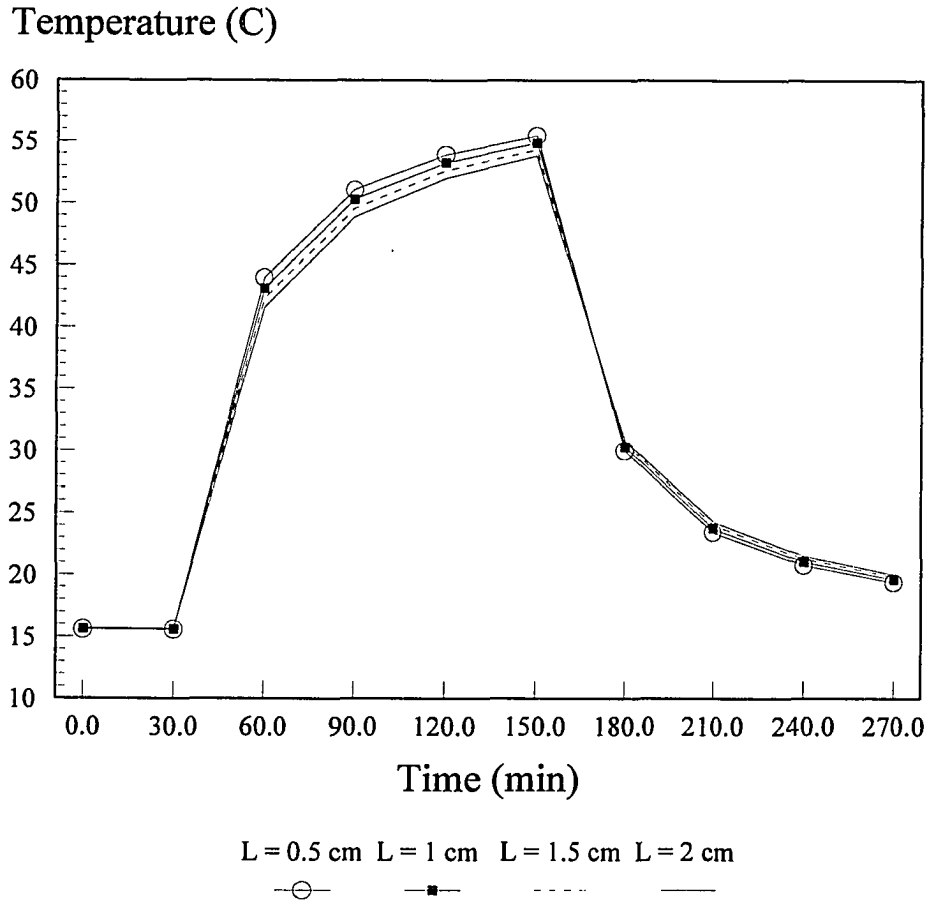


Figure 2-2
Modified mathematical model of step function heating source with a finite plastic object buried under sand at different buried depths (L = 0.5 cm, 1 cm, 1.5 cm and 2 cm). The heating time is 2 hours.

calculation in Figure 1-6 and Figure 1-9, as well as in experiments in Figure 1-14 and Figure 1-15, respectively. Comparing the results from Figure 2-1 and Figure 2-2 with the results from Figure 1-14 and Figure 1-15, it can been seen that after modification the mathematical model can better express the experimental results. First, the surface temperature will eventually become uniform after the radiation switched off for several hours. Second, the temperature changing rate at the beginning of the radiation switched on and off was greater than before modification. After several computations, we found that among these factors (thermal properties, size and buried depth of the object ) related with $FB_n$, the objects' side flux, the thermal properties of the object will strongly affect the flux of $FB_n$.

More experiments need to be done to get more statistical data for verifying the relationship of $FB_n$ with the object's thermal properties. If we only consider the surface temperature on the top of the buried object's center point, the results can be significant a guide for further studies.

## 3.3 The temperature distribution on the surface with a buried finite object

### 3.3.1 Mathematical calculation

The mathematical model we discussed previously can better explain the surface temperature of the central area over a finite buried object. Acturaly, as a finite sized object buried, the thermoisopleth will show on the surface; that will help to distinguish the regular shape of man-made objects from irregular shaped natural objects, like rocks. So we are going to seek the temperature distribution on the surface mathematically.

As discussed previously, after an object is buried, the temperature above it will change according to its material and the thickness of the object and its buried depth. Or, we can say that the effect that a buried object has on the surface is, it changes the thermal properties in the vicinity. The relationship of sand's thermal inertia to the object's thermal inertia and the effective surface thermal inertia is given by Watson [13].

According to the heat conduction law, if we assume the buried object has a finite size, its depth is D and the buried distance from the surface is L, the effective thermal conductivity $K_e$ on its vicinity will be [17]:

$$K_e = \frac{K_1 K_2 (L + D)}{K_1 \times D + K_2 \times L} \tag{2.2}$$

Here, $K_1$ is thermal conductivity of covered layer and $K_2$ is thermal conductivity of a buried object.

Assuming that the soil is homogeneous, in the absence of any buried objects, the temperature of the surface is uniform at any observation time; the temperature is dependent only on time and the thermal properties of the soil. If an object is then buried under the soil, the surface temperature in the central area of its vicinity can be expressed by modified mathematical model. The isothermal contours around the vicinity of buried object corespond to the shape of the object, and their values depend on the size and thermal properties of the object and the depth at which it is buried. If a cylindrical object with a radius of "a" and depth of D is buried under ground at depth L, the thermal properties of the surface on the same area S1 can be numerically equivalent to $P_e$, $K_e$, $k_e$, $\rho_e$, which depends on the property of the material of the object. The diffusion equations

of the temperature distribution on the surface of the ground in the presence of a finite size object buried are [12]:

$$\frac{\partial^2 v_e}{\partial r^2}+\frac{1}{r}\frac{\partial v_e}{\partial r}-\frac{1}{k_e}\frac{\partial v_e}{\partial t}=0 \qquad 0<r<a,\ t>0 \qquad (2.3)$$

$$\frac{\partial^2 v_1}{\partial r^2}+\frac{1}{r}\frac{\partial v_1}{\partial r}-\frac{1}{k_1}\frac{\partial v_1}{\partial t}=0 \qquad x>0,\ t>0 \qquad (2.4)$$

Assumed initial condition are: 1) for 0<r<a, the surface temperature is constant and equal to that of the surface temperature in the central area of object's vicinity, as t=0; 2) when r>a, the surface temperature is constant and equal to that with no buried object as, t=0; 3) also assuming that there is no contact resistance at the surface of separation x=0, the boundary conditions are:

$$K_e\frac{\partial v_e}{\partial r}=K_1\frac{\partial v_1}{\partial r} \qquad r=a,\ t>0 \qquad (2.5)$$

$$v_e=v_1 \qquad x=0,\ t>0 \qquad (2.6)$$

Using Laplase transfer function [12], the temperature distribution on the surface is:

$$v_e=V_1^{'}+\frac{4K_eK_1k_1(V_e^{'}-V_1^{'})}{a\,\pi^2}\int_0^{\infty}\frac{e^{-k_eu^2t}\,J_1(au)J_0(ru)}{\Phi^2(u)+\Psi^2(u)}du \qquad (2.7)$$

$$v1 = V_1' + \frac{2K_e k_1^{1/2}\left(V_e' - V_1'\right)}{a\ \pi^2}\int_0^{\infty}\frac{e^{-k_e u^2 t}}{u}\frac{J_1(au)\left[J_0(kru)\Psi(u) - Y_0(kru)\Phi(u)\right]}{\Phi^2(u)+\Psi^2(u)}du \tag{2.8}$$

$$\Phi(u) = K_e k_1^{1/2} J_1(au) J_0(kau) - K_1 k_e^{1/2} J_0(au) J_1(kau) \tag{2.9}$$

$$\Psi(u) = K_e k_1^{1/2} J_1(au) Y_0(kau) - K_1 k_e^{1/2} J_0(au) K_1(kau) \tag{2.10}$$

Figure 2-3 gives the calculated surface temperature distribution of a finite object (plastic) buried under the sand at depths of 1 cm, 2 cm, and 4 cm under diurnal conditions at the local time 14:30. Figure 2-4 gives the calculation results under the same conditions at the local time 6:00 am. We can see from Figure 2-3 and Figure 2-4 that the temperature distribution is a function of the depth of the buried object. As the depth increases, the temperature near the center becomes lower, and the slope become less sharp. These temperature distribution contain the thermal information of not only the shape of the objects but their buried depths also.

Figure 2-5 gives such a simulated surface temperature distribution of a finite object (plastic) buried under the sand at 0.5 cm, 1 cm, 1.5 cm and 2 cm depths under lamps-on condition after 30 minutes of radiation. From the simulations, it is clear that as the depth increase, the temperatures near the center become lower, and the temperature gradients become more gradual. Practically, this will results in a smearing of the temperature contours in the vicinity of the buried object.

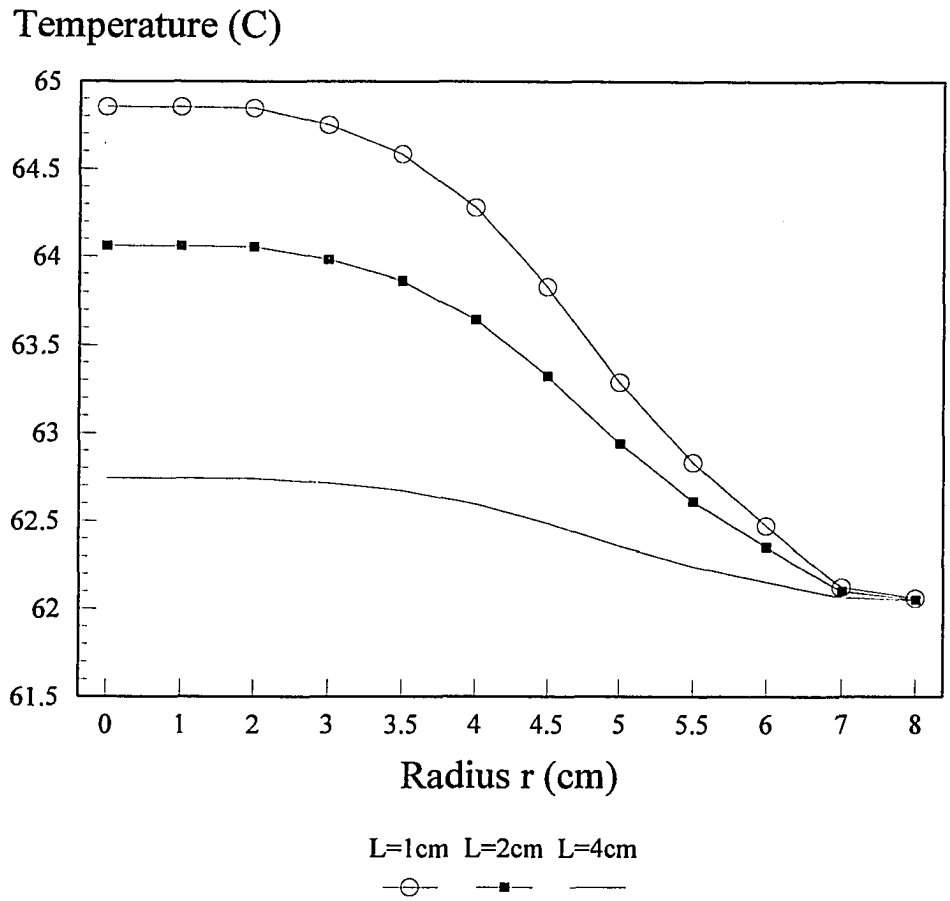


Figure 2-3
Temperature distribution on the surface of sand with a finite plastic Object buried at L = 1 cm, 2 cm and 4 cm. Heating source is diurnal solar. Local time 14:30.

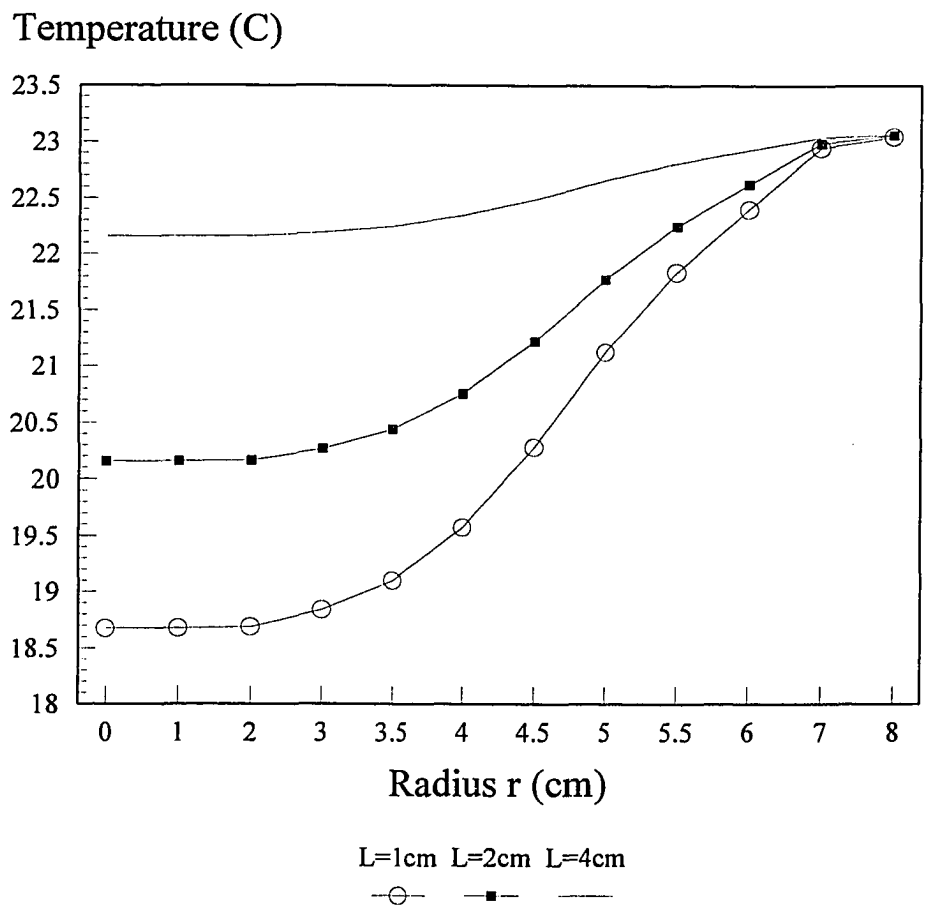


Figure 2-4
Temperature distribution on the surface of sand with a finite plastic object buried at L = 1 cm, 2 cm and 4 cm. Heating source is diurnal solar. Local time 6:30.

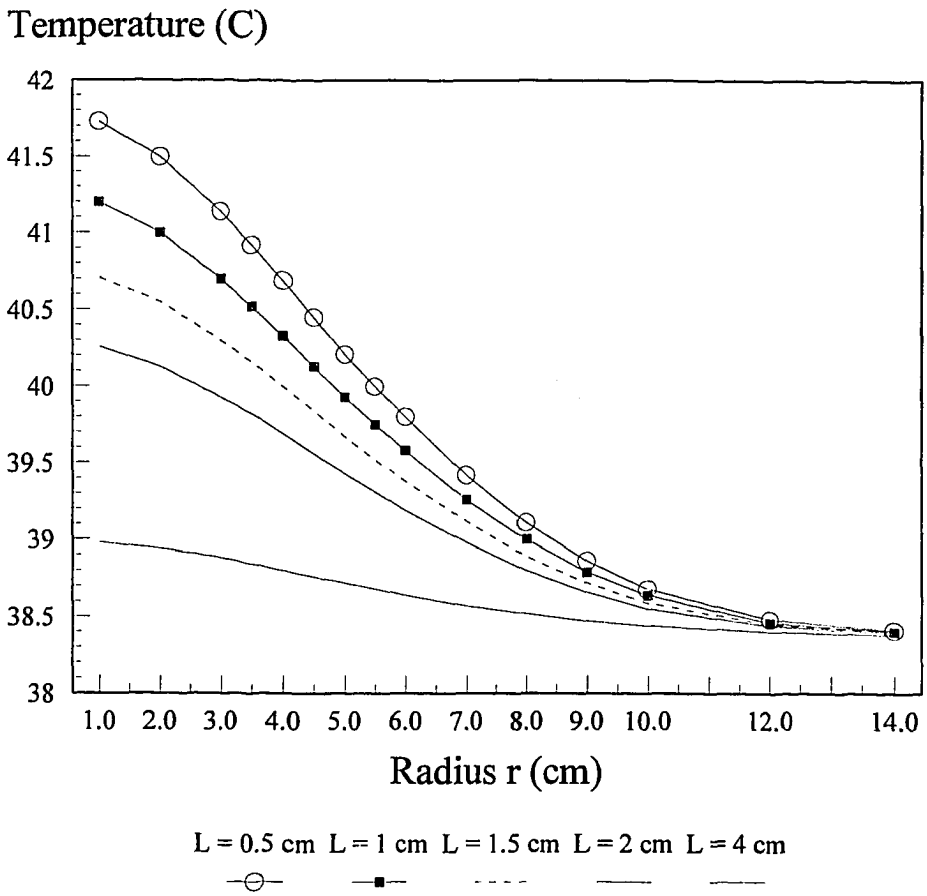


Figure 2-5
Temperature distribution on the surface of sand with plastic object buried at different dept. Heating source is a step function heating source, after 30 minutes heating.

3.3.2 Experiment results and discussion

Figure 2-6 shows a sample image of the experiment conducted July 30, 1993 with a round plastic object, 4 1/2" in diameter and 2 1/2" thick buried at 3/4"' depth. The image was taken after 20 minutes of lights on. The contours of temperature distribution surrounding the buried object can clearly be seen and its shape is nearly round. In the image, there are temperature changes in some areas where nothing is buried beneath, possibly because of sand density and /or sand moisture. These contours form an irregular shape. Figure 2-7 shows the temperature distribution of one line across the object, (the line showed in Figure 2-6). In the center of the plastic object, the temperature is approximately equal to the value of the modified mathematical model. As the distance from the center increases, the temperature gradually decreases to that of the sand temperature. The rate of decrease will depend on the buried depth of the object.

Figure 2-8 plots the radial temperature distribution on the surface of the sand over plastic objects buried at different depths (0.5 cm, 1 cm, 1.5 cm and 2 cm, same as the experiments of May 28, to May 31, 1994.) after 30 minutes of a radiation source switched on. As we mentioned in Part One, the isothermal patterns in the sand above the buried objects reflect their shapes. The deeper the objects are buried, the more diffuse the isotherm patterns are. The temperature distribution lines in Figure 2-8 also show that as the depth increases, the temperatures near the center become lower, and the temperature gradients become more gradual. These results are in qualitative agreement with the simulations in Figure 2-5.

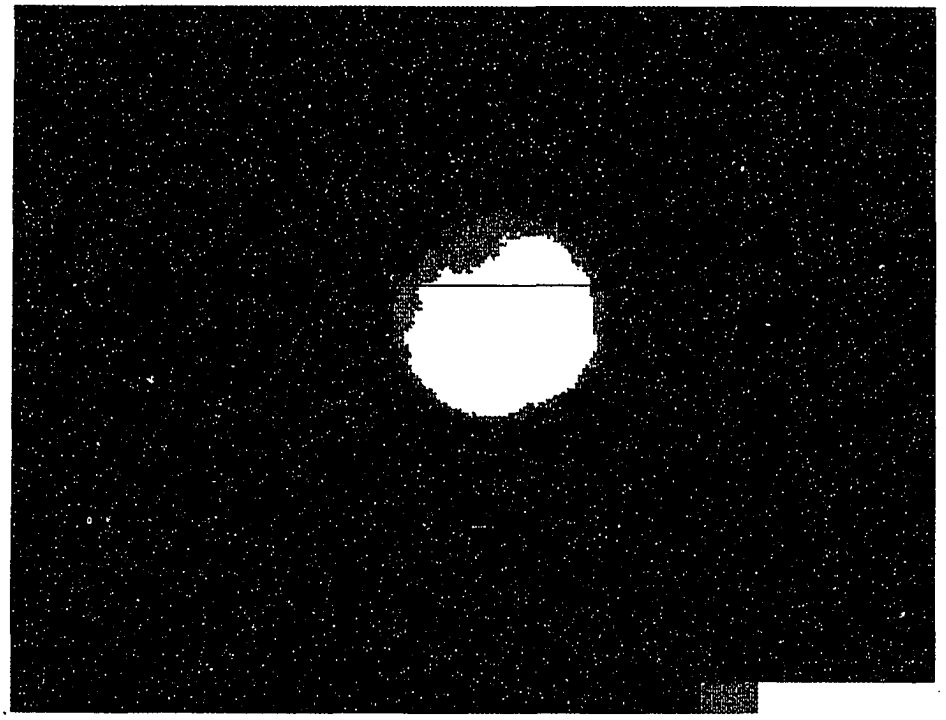

Figure 2-6
A sample thermal image of a plastic object buried at 1 cm, heated by a step function radiation, for 2 hours. The image was taken 20 minutes after radiation was switched on.

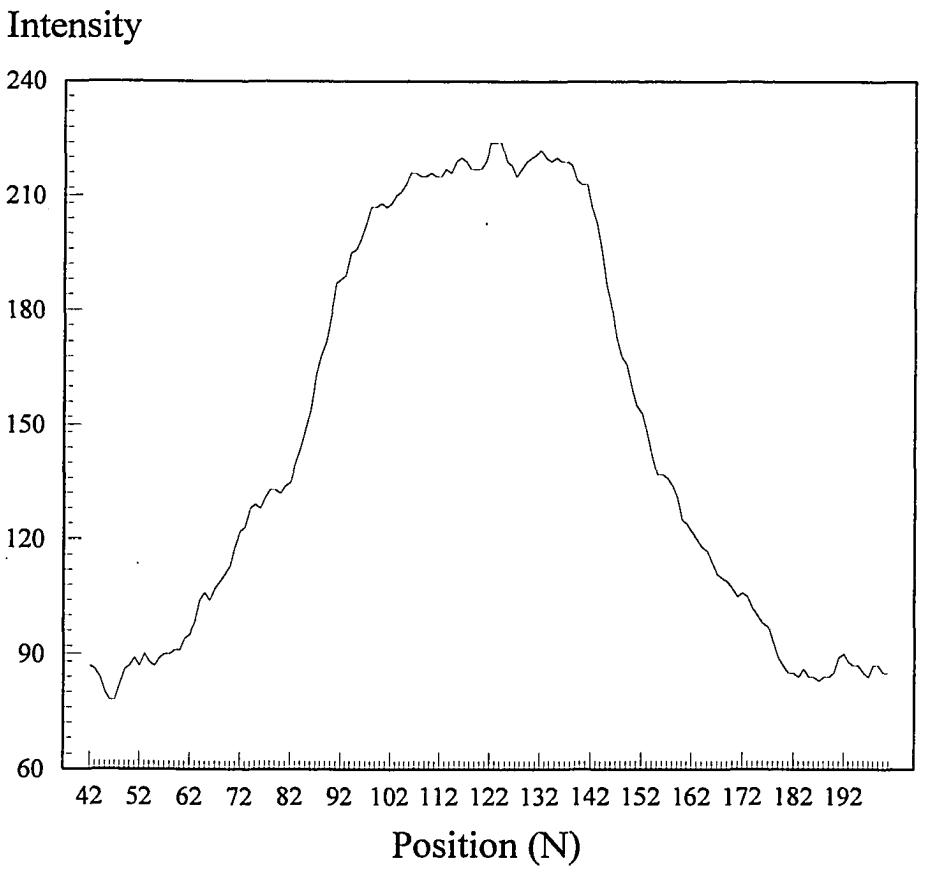


Figure 2-7
Temperature distribution on the surface of sand along the line shown in Figure 2-6.

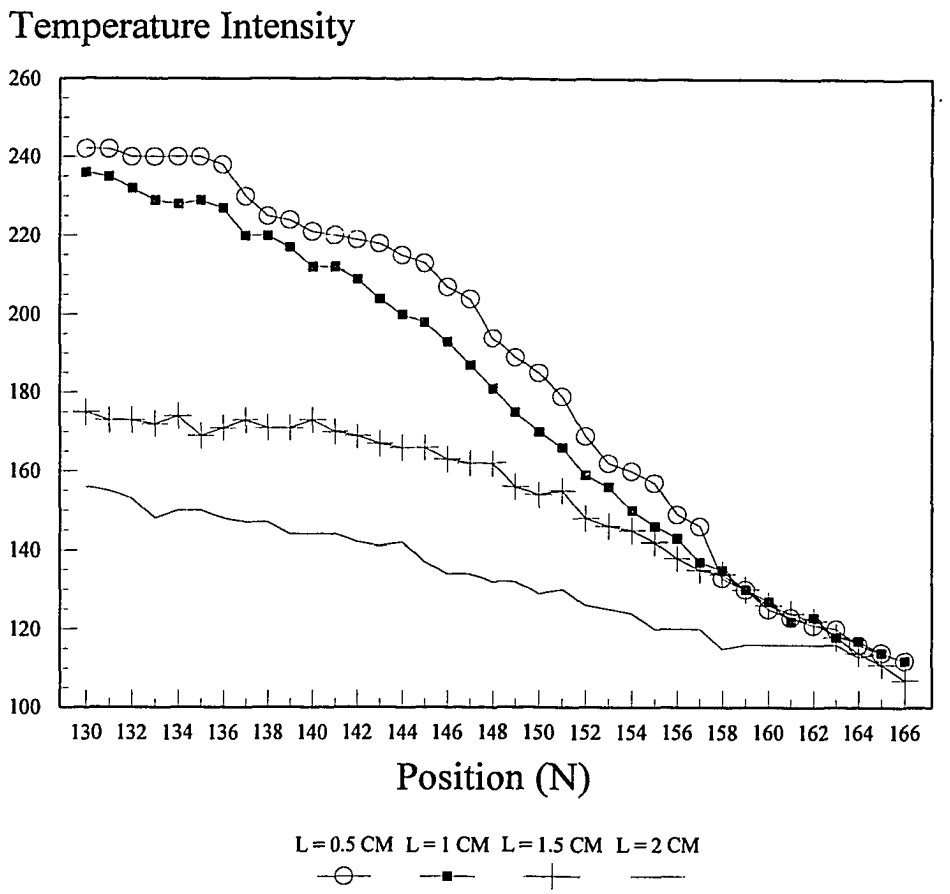


Figure 2-8
Temperature distribution on the surface of sand with a plastic object buried at different depths heated by a step function heating source for 30 minutes.

## 3.4 Further image and data processing

### 3.4.1 The processing of the images

A further clarifying step in images processing is the subtraction of an image taken during the heating cycle from that taken during the cooling cycle. This process enhances the temperature differences and removes the visual background "noise" in the thermal images. As seen in Figure 1-13, there were temperature changes even in the areas where nothing was buried under the surface, possibly due to sand density and/or sand moisture.

Here we measured only metal and plastic objects which were separately buried to see how any of the background "noise" affected their detection. Figure 2-7 and 2-8, show the infrared images of a 3" round by 1" thick piece of aluminum buried at a depth of 1 cm, heated about 1 hour and cooled for 1 hour. Figure 2-7 shows an image taken during the heating cycle showing a low temperature over the metal, and a higher temperature around it. The temperature differences of the surrounding area is clear to see, where the temperature contours do not conform to any particular shape. Figure 2-8 shows that the temperature above the metal area is higher than the surrounding area during the cooling cycle. And it is a big difference in temperature distribution in the surrounding area. However this time, it can be seen that the surrounding area has a higher temperature during heating cycle it still maintains a higher temperature during the cooling cycle. As show in Figure 2-9, subtracting two images from the heating and the cooling cycles result in removing almost all background noise, making the contour of the metal object very clear. The contours retain their shape so that geometric object recognition and contouring remains available.

If there is a plastic object buried underground which shows a higher temperature than the surrounding area during the heating cycle and a lower temperature during the

Figure 2-9
Infrared image taken during the heating cycle of the surface of the sand that contains a piece of round metal.

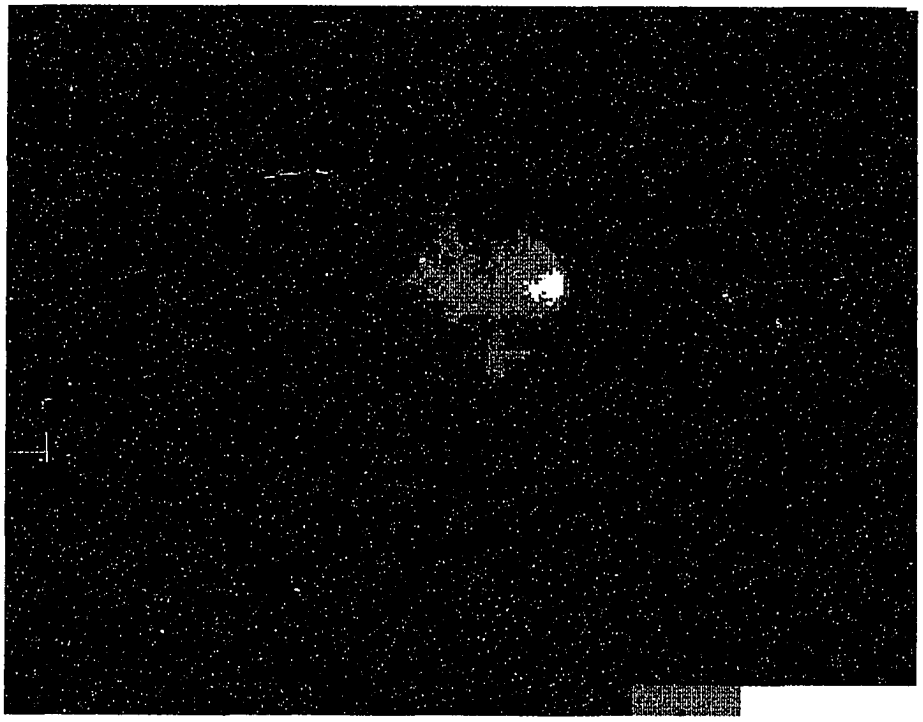

Figure 2-10
Infrared image taken during the cooling cycle of the surface of the sand that contains a piece of round metal.

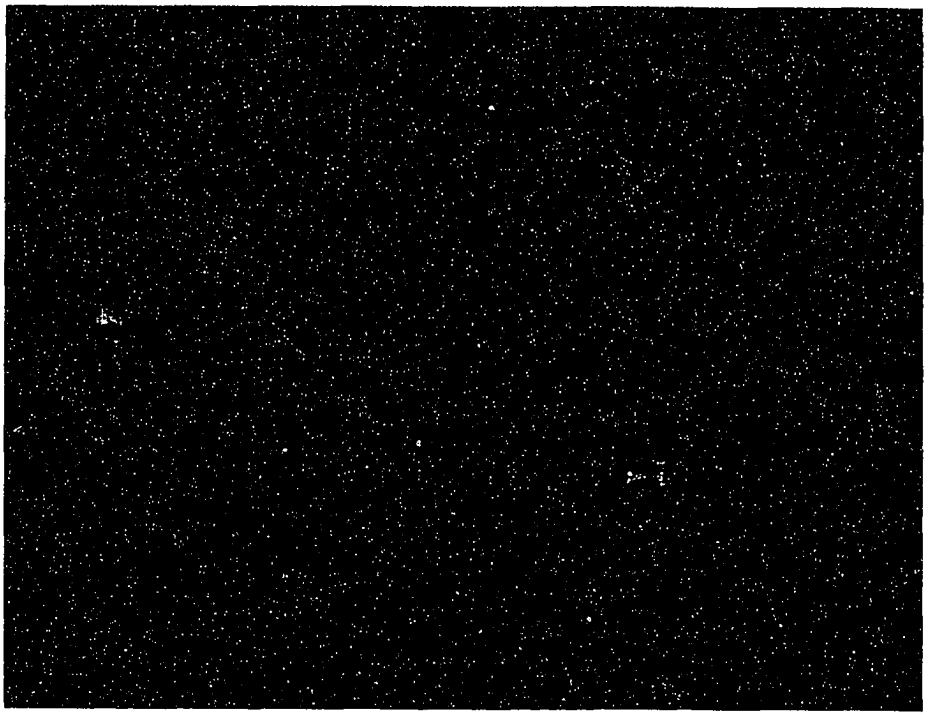

Figure 2-11
The resulting image of a buried round metal object when mathematical values of the cooling cycle are subtracted from the mathematical values of the heating cycle. Heat is a step function source.

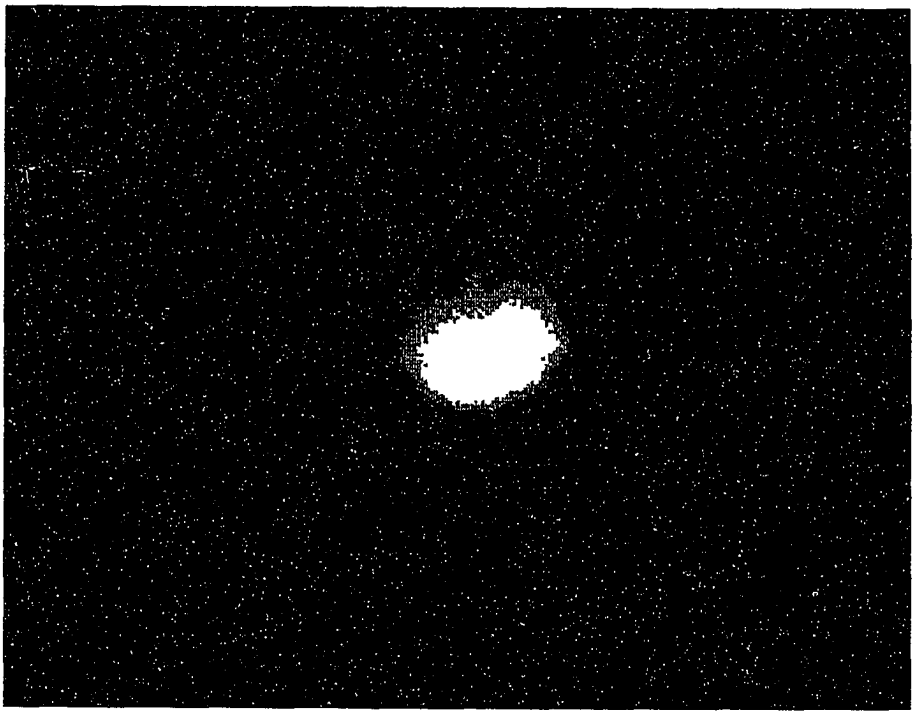

Figure 2-12
The resulting image of a buried round plastic object when mathematical values of the cooling cycle are subtracted from the mathematical values of the heating cycle. Heat is a step function source.

cooling cycle, the contour remaining after subtracting the heating image from the cooling image will still been seen.

3.4.2 The processing of the data from the infrared images

From theoretical study and experimental examination, it is clear that the sudden change of the surface flux by turning a step function radiation on and off can generate various rates of differential temperature changes on the surface which depend on the buried materials under the surface and the buried distances. In practice, we can visually recognize and differentiate the above objects in less than a few minutes during either cooling and / or heating based on the rate of movement of isothermal contours in the vicinity of the buried objects. To this end, it will be useful to generate real time images of the rates of change of temperature. In order to do real time recognition, the characteristic of the temperature change rate by the different material and their depth need to be studied.

We recorded the temperature changes of the surface over various objects during the first 20 minutes when the heating and cooling cycle started (step function radiation switched on and off), in Figure 3-13 (in the heating cycle) and Figure 3-17 (in the cooling cycle). These data were collected from the experiment on July 30, 1993: a plastic, rock and metal object buried under the sand at the depth of 0.3 cm, heated by a step function radiation for 4 hours. The time interval between each data collected was 2 minutes. A great temperature change was noted during this period.

The temperature differences between each object buried and the sand only area were showed in Figure 2-14 in the heating cycle and Figure 2-18 in the cooling cycle. Where,

$$\Delta T(t) = T_{object}(t) - T_{sand}(t) \qquad (2.11)$$

$\Delta T(t)$ is the temperature difference at the time t, $T_{object}(t)$ and $T_{sand}(t)$ is the temperature in the vicinity of a buried object and the sand only at time t. It is not surprise to see that the temperature difference of plastic is positive in heating cycle and negative in cooling cycle; and it is greater in value than the other cases.

The speed of absolute temperature changes in the vicinity of a buried object and the sand only were given in Figure 2-15 and Figure 2-19. Where the speed of temperature changes Tp ( t ) is:

$$T_p(t) = \left| \frac{dT_{object}(t)}{dt} \right| \tag{2.12}$$

$T_{object}(t)$ is the surface temperature of each buried objects or sand only at time t.

The acceleration of absolute temperature changes on the area of the vicinity of a buried object and the sand only were given in Figure 2-16 ( in heating cycle ) and Figure 2-20 ( in cooling cycle ). Where the acceleration of temperature changes Ta ( t ) is:

$$T_a(t) = \left| \frac{dT_p(t)}{dt} \right| \tag{2.13}$$

or,

$$T_a(t) = \left| \frac{d^2T_{object}(t)}{dt^2} \right| \tag{2.14}$$

Both speed and acceleration of temperature change of each object showed a great value in the first 10 minutes in the heating and the cooling cycles and reflected the thermal characteristic of the buried objects, the lower thermal property is, the greater speed and acceleration of temperature change ( like plastic ). And it is also shown that the speed and acceleration for a buried object are almost the same in either the heating or the cooling

cycle, which further proved that they are the function of the object's thermal characteristics.

Figures 21 to Figure 26 present the surface temperature, the speed and the acceleration of the surface temperature of a plastic object buried at different depths (0.5 cm, 1 cm, 1.5 cm and 2 cm. Experiments performed May 28 to 31, 1994) in the heating and the cooling cycles. They are showed the information of buried depth of a object can also find in the value of speed and acceleration of the temperature changes.

Since the speed and acceleration of temperature changes can better represent the thermal characteristics of the buried objects and depth and they show great values in the first 10 minutes when the radiation changes, it is sure that along with observing the surface temperature, the calculating of the temperature differences between the objects buried and the sand surface, and the speed and acceleration of the temperature changes will enhance the real time detection.

## 3.5 Summary

A mathematical model derived from the equation of heat conduction, and modified by the experimental results, was developed as an approach to interpret the thermal infrared information on the surface of the ground with a finite size object buried beneath and heated by an artificial step function radiation. The flux on the surface of the step function radiation source was measured using a power meter and applied to the mathematical model for numerical calculation of surface temperature. When considering the finite size of the object, the object's related surface flux should be included in the total

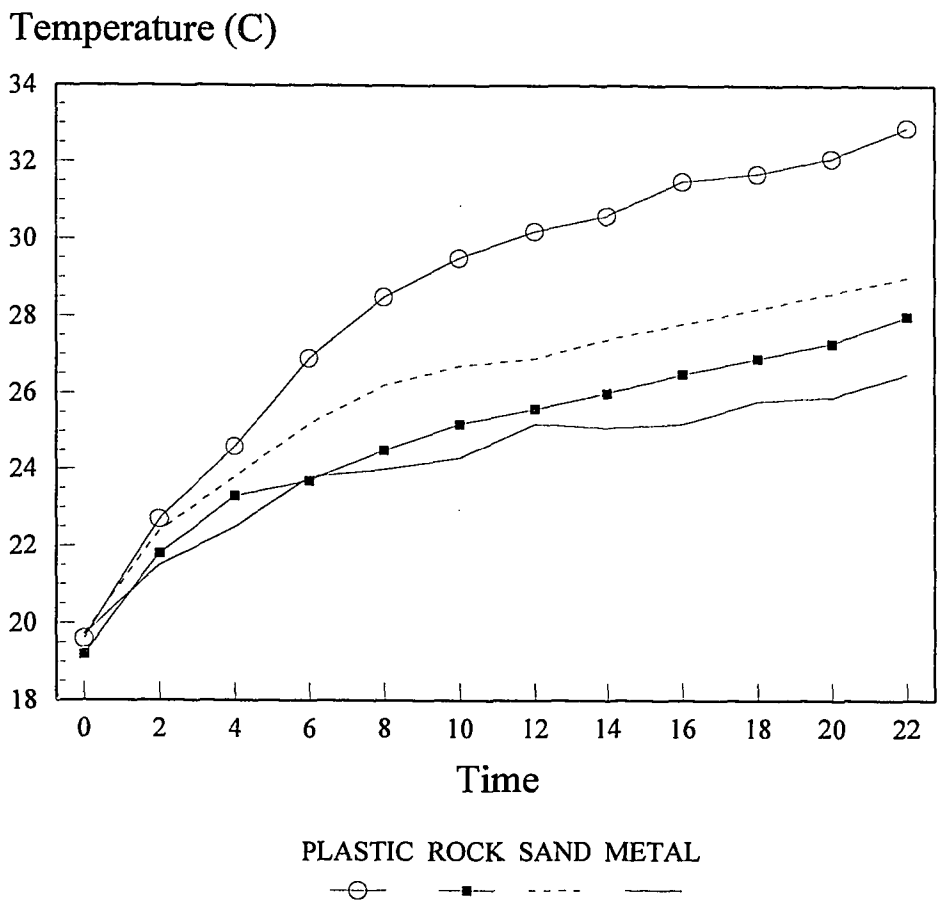


Figure 2-13
Surface temperature ( in heating cycle ) of plastic, rock and metal objects buried under sand. Data collected from experiment on July 30, 1993.

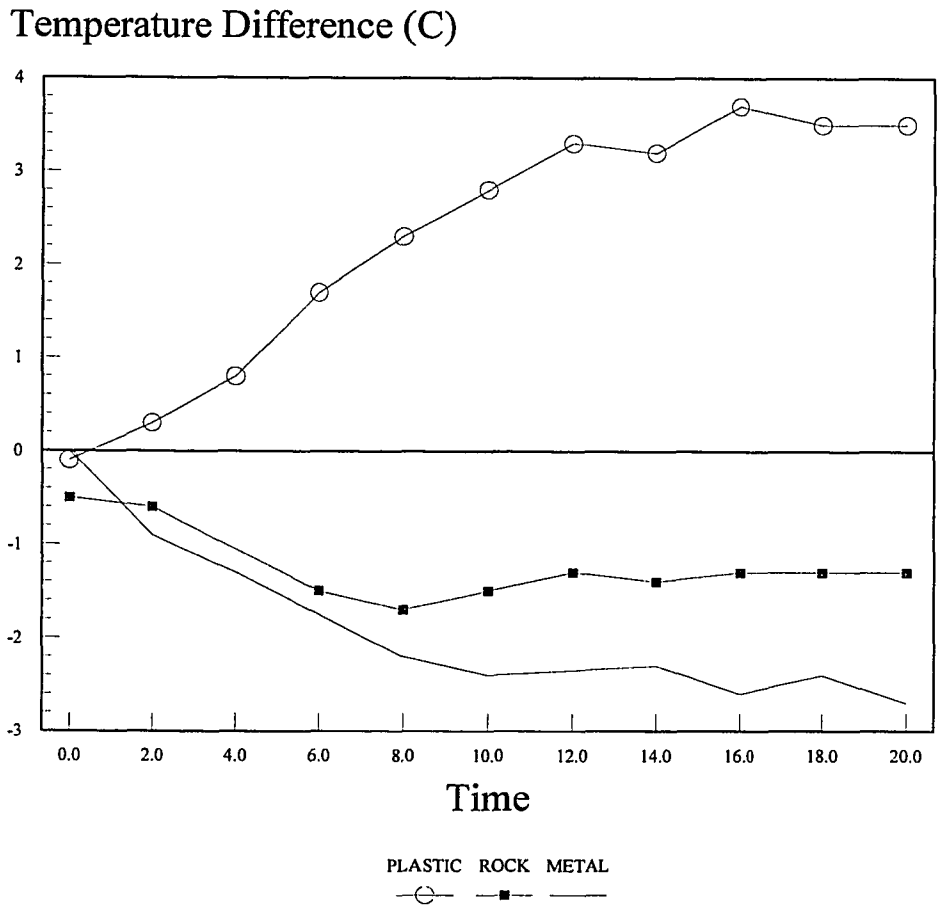


Figure 2-14
Surface temperature differences of a plastic, rock and metal object buried under sand to the sand-only area, at the first 20 minutes of radiation turned on. Data collected from experiment on July 30, 1993.

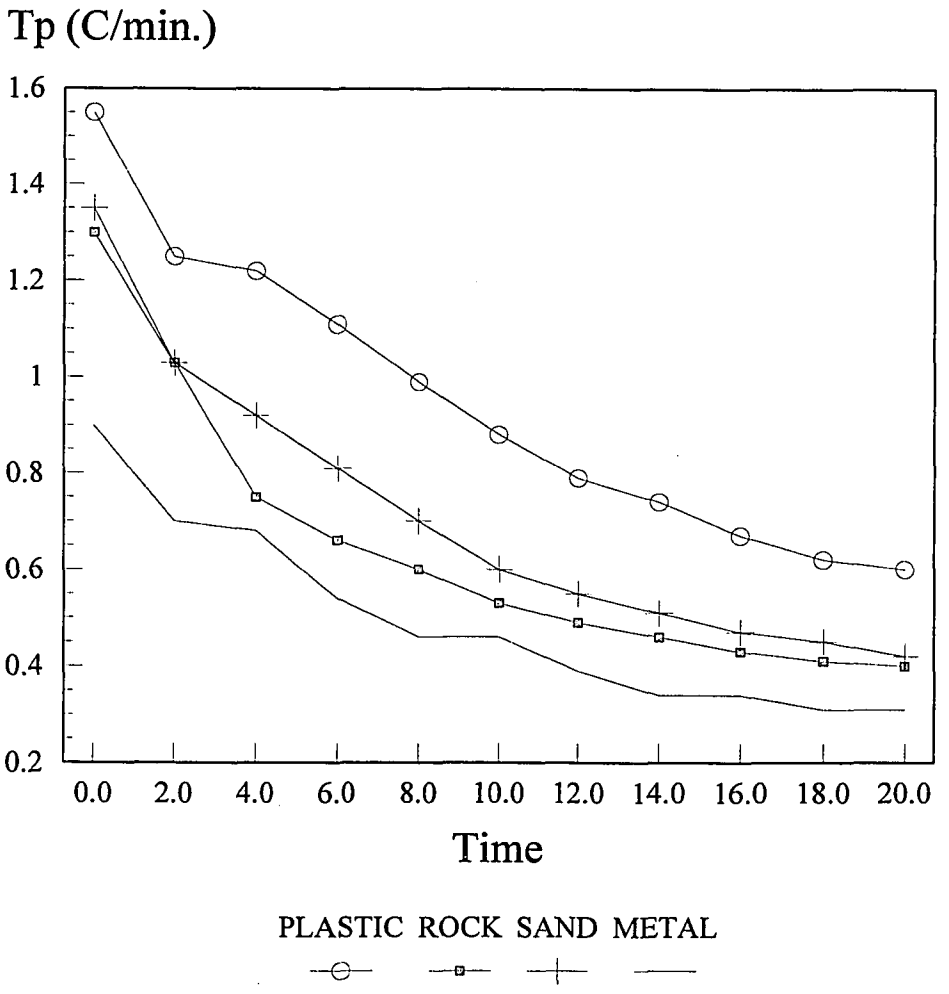


Figure 2-15
The speed of surface temperature changes in the vicinity of buried objects (plastic, rock and metal) and the sand-only area, in the first 20 minutes of radiation switched on. Data collected from experiment on July 30, 1993.

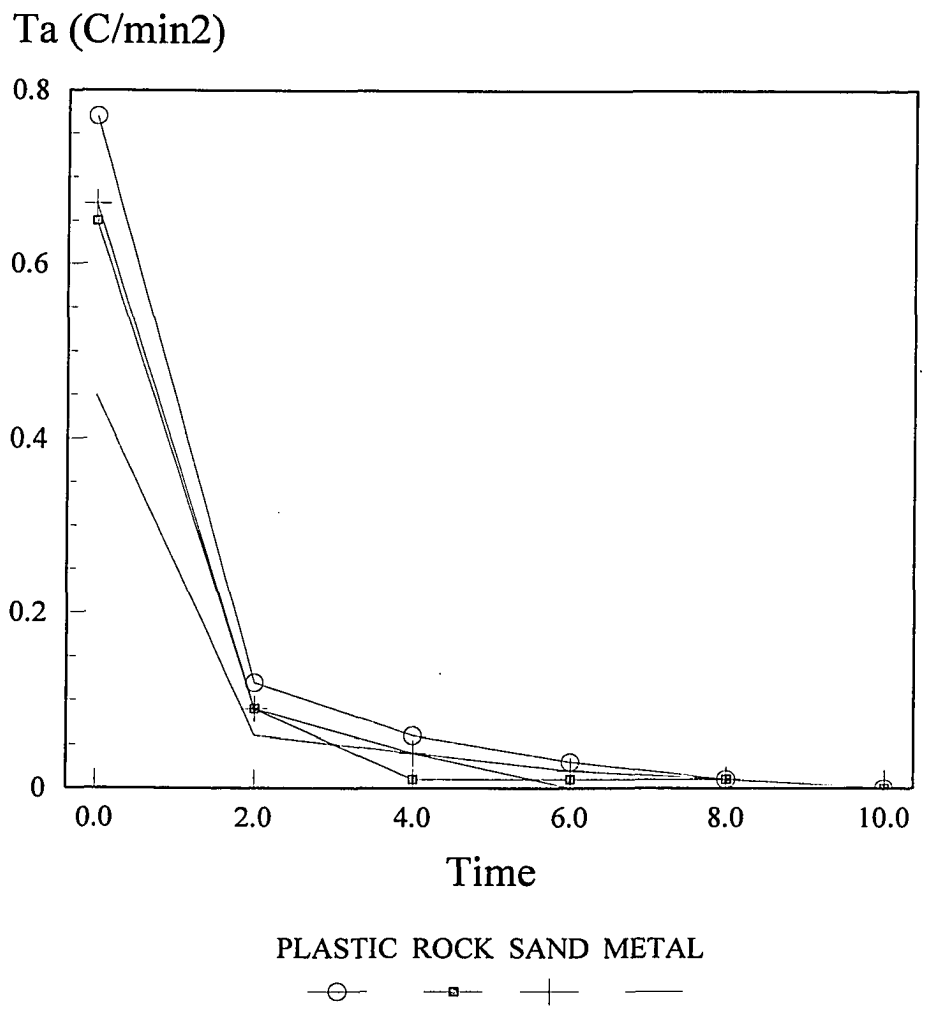


Figure 2-16
The acceleration of surface temperature changes in the vicinity of buried objects (plastic, rock and metal) and the sand-only area, in the first 20 minutes of radiation switched on. Data collected from experiment on July 30, 1993.

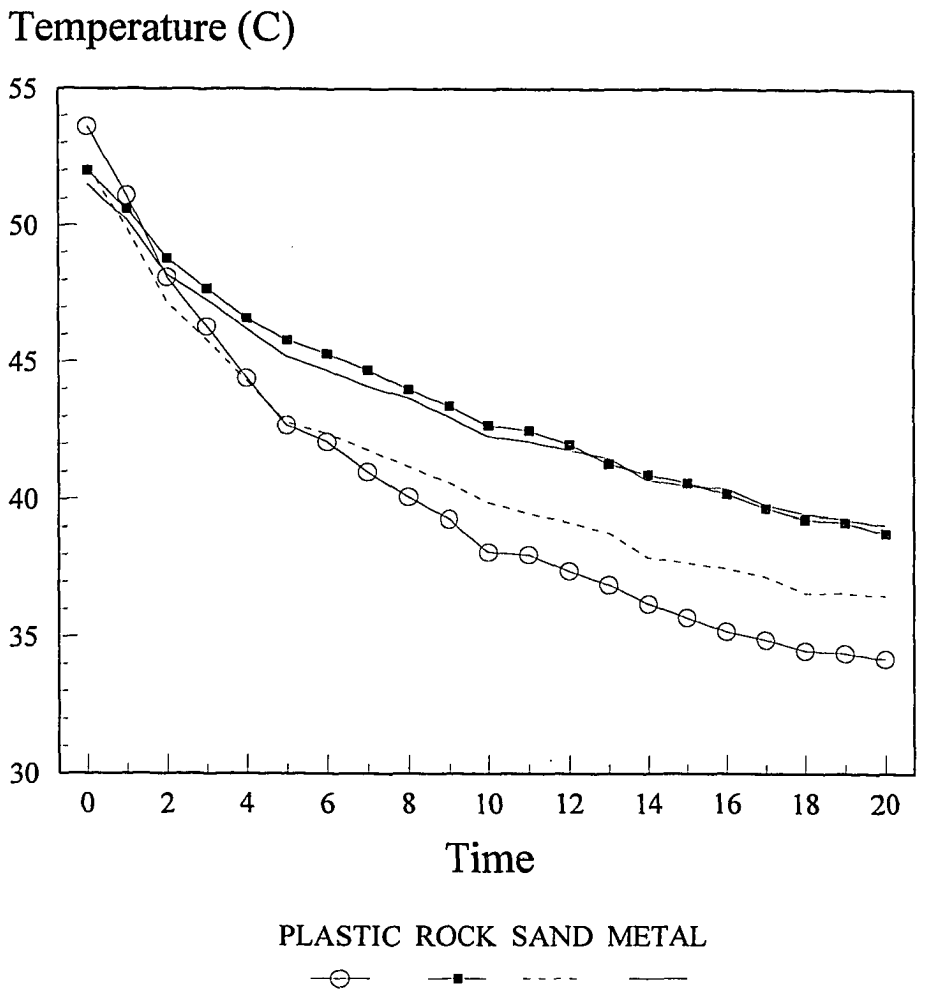


Figure 2-17
Surface temperature with plastic, rock and metal objects buried under sand.
Data collected from experiment on July 30, 1993 ( in cooling cycle ).

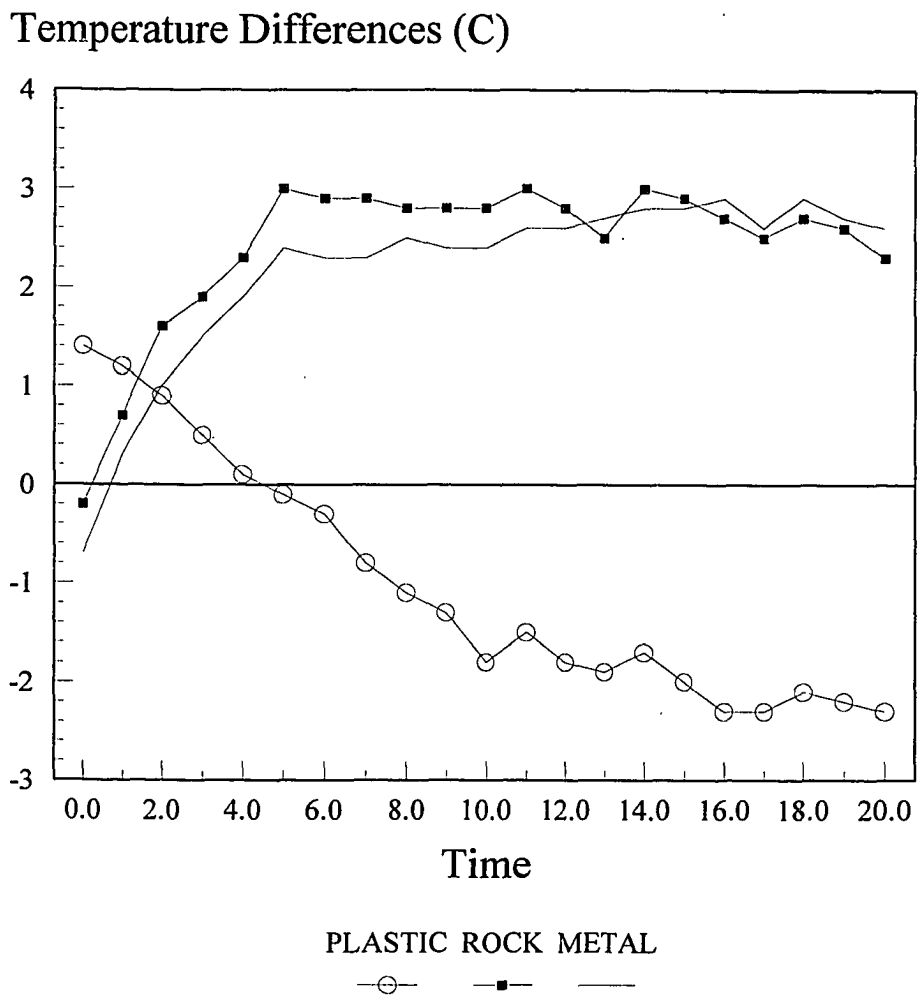


Figure 2-18
The surface temperature differences of a plastic, rock and metal object buried under sand and the sand-only area, in the first 20 minutes of radiation turned off. Data collected from experiment on July 30, 1993.

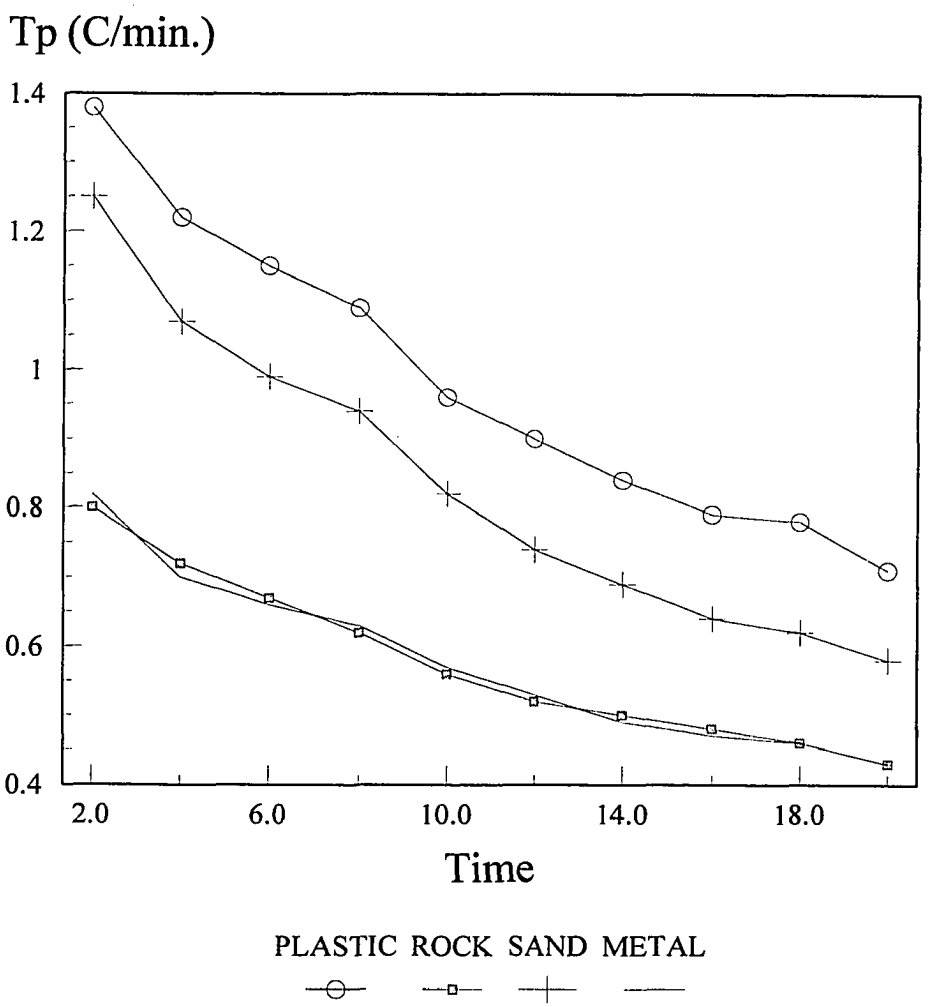


Figure 2-19
The speed of surface temperature changes in the vicinity of buried objects (plastic, rock and metal) and the sand only area, in the first 20 minutes when radiation switched off. Data collected from experiment on July 30, 1993.

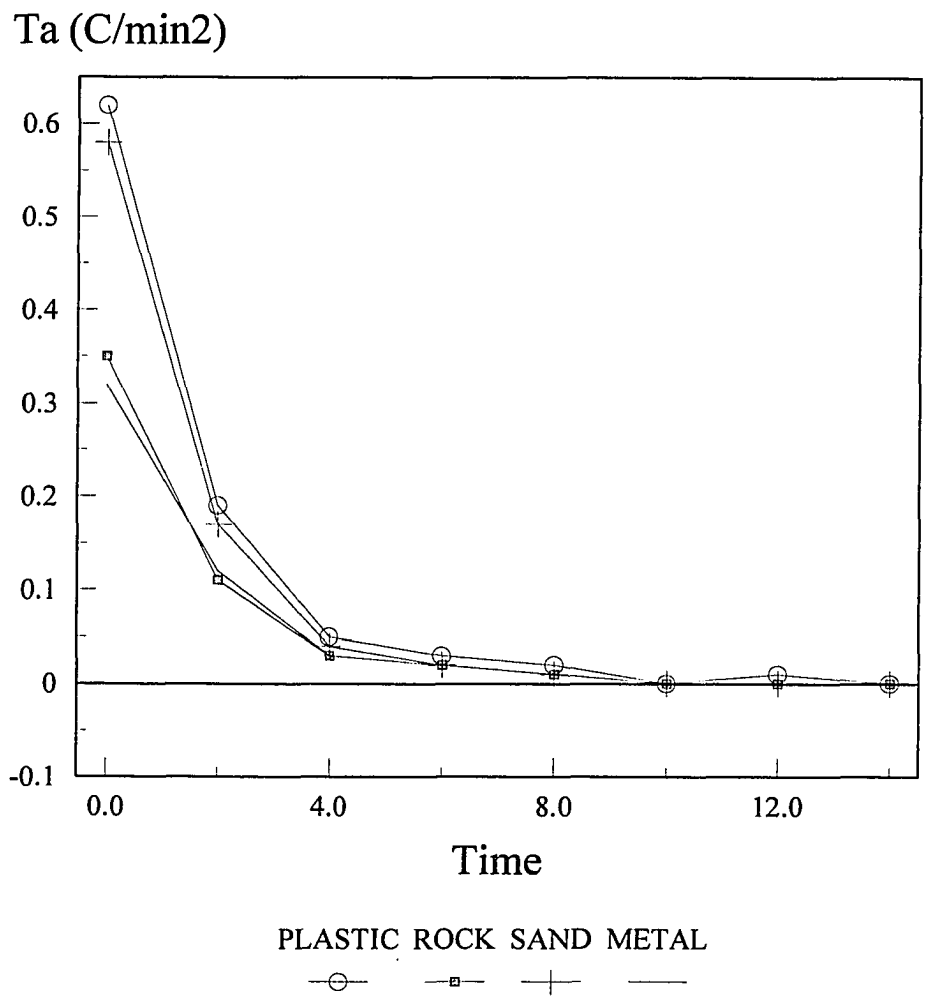


Figure 2-20
The acceleration of surface temperature changes in the vicinity of buried objects (plastic, rock and metal) and the sand-only area, in the first 20 minutes when radiation switched off. Data collected from experiment on July 30, 1993.

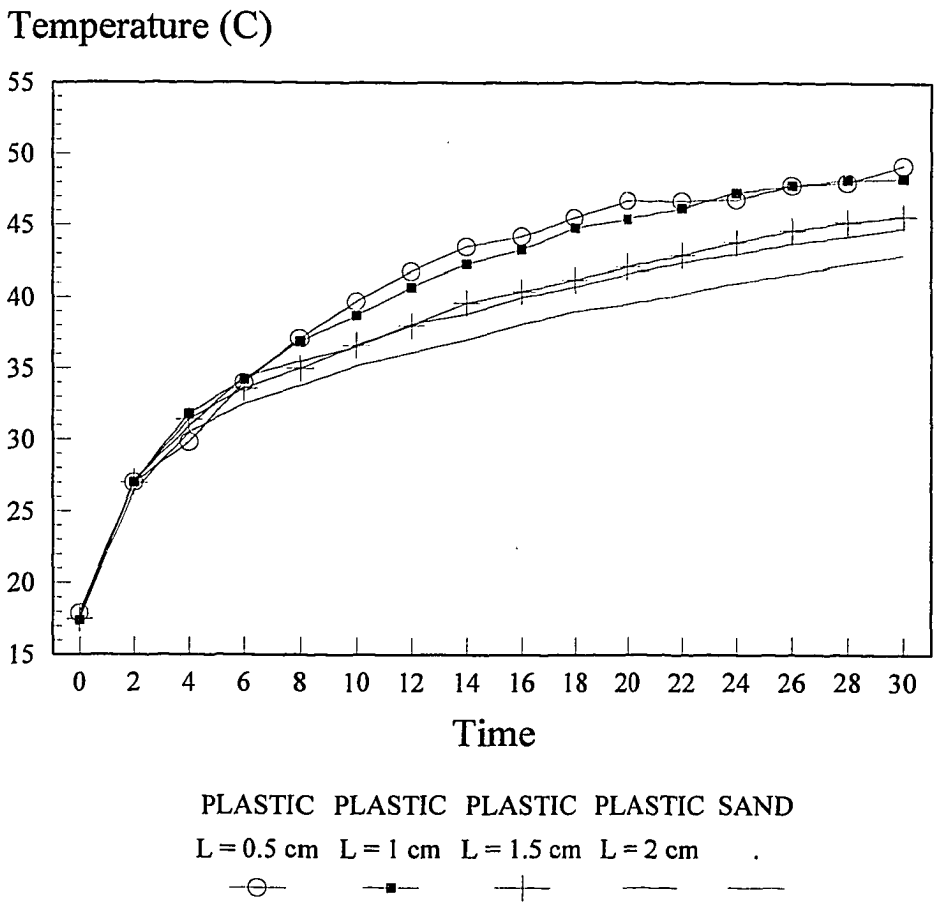


Figure 2-21
Surface temperature with a plastic object buried under sand at depths L=0.5 cm, 1 cm, 1.5 cm and 2 cm.

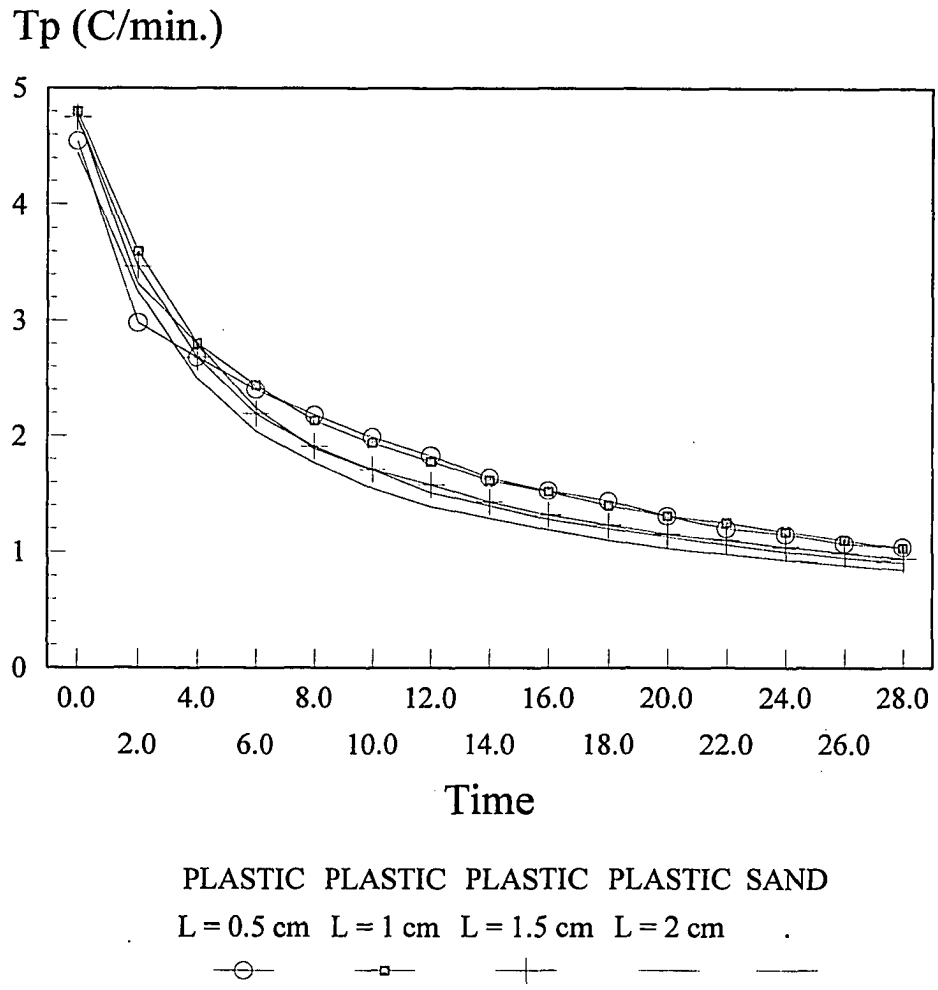


Figure 2-22
The speed of surface temperature changes on the vicinity of a plastic object buried under sand at depth L=0.5 cm, 1 cm, 1.5 cm and 2 cm and the sand only area, in the first 20 minutes when radiation switched on.

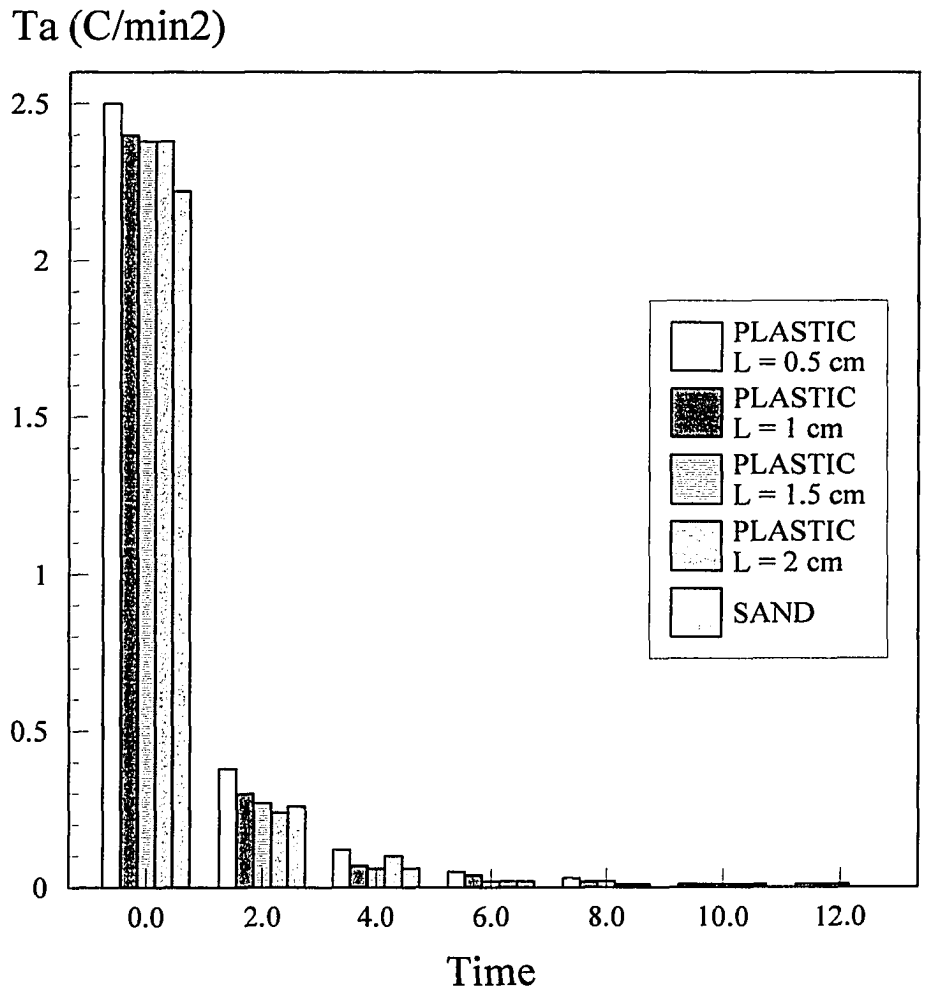


Figure 2-23
The acceleration of surface temperature changes in the vicinity of a plastic object buried under sand at depth L=0.5 cm, 1 cm, 1.5 cm and 2 cm and the sand-only area, in the first 20 minutes when radiation switched on.

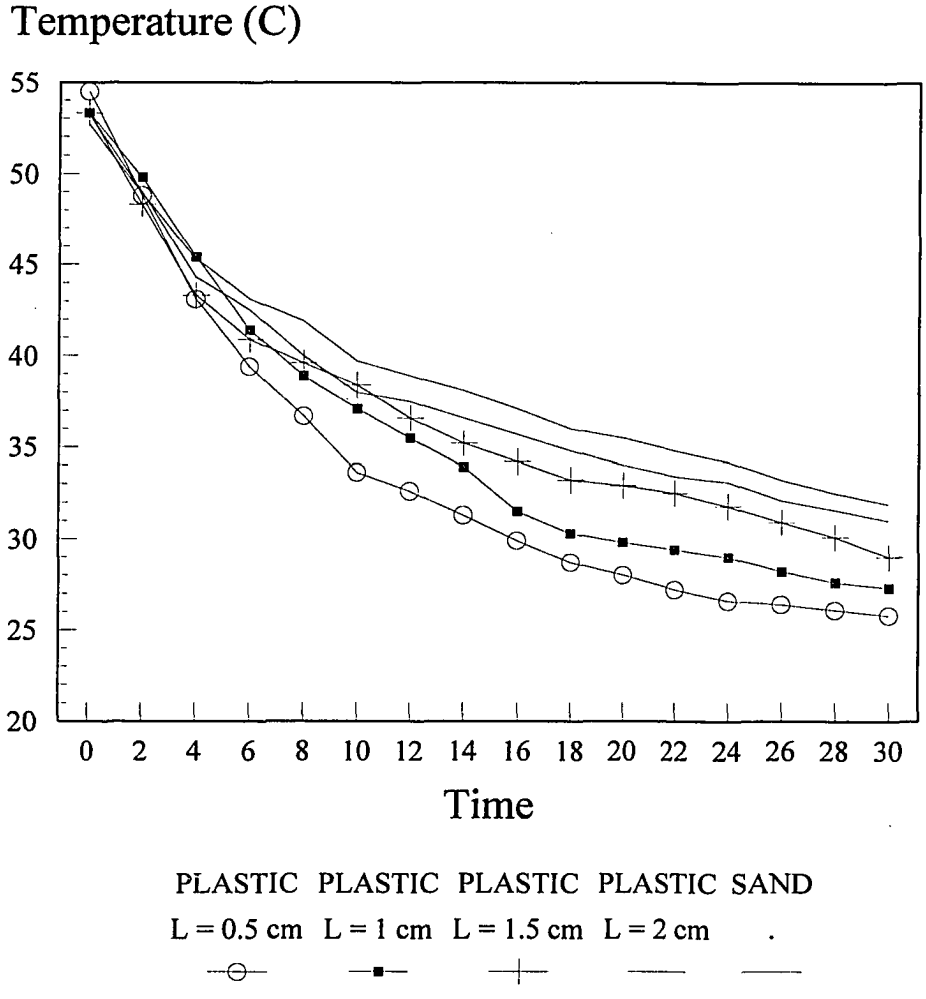


Figure 2-24
Surface temperature with a plastic object buried under sand at depths L=0.5 cm, 1 cm, 1.5 cm and 2 cm. ( during cooling cycle ).

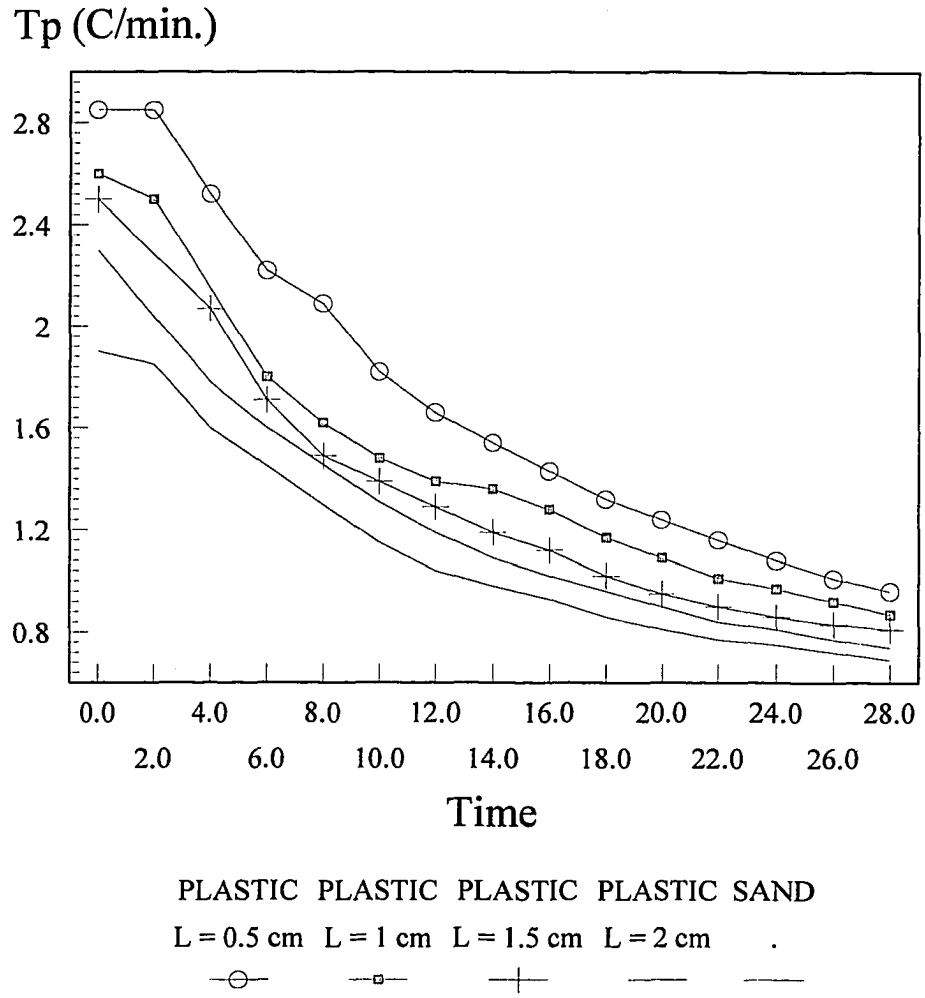


Figure 2-25
The speed of surface temperature changes in the vicinity of a plastic object buried under sand at depth L=0.5 cm, 1 cm, 1.5 cm and 2 cm and the sand-only area, in the first 20 minutes when radiation switched off.

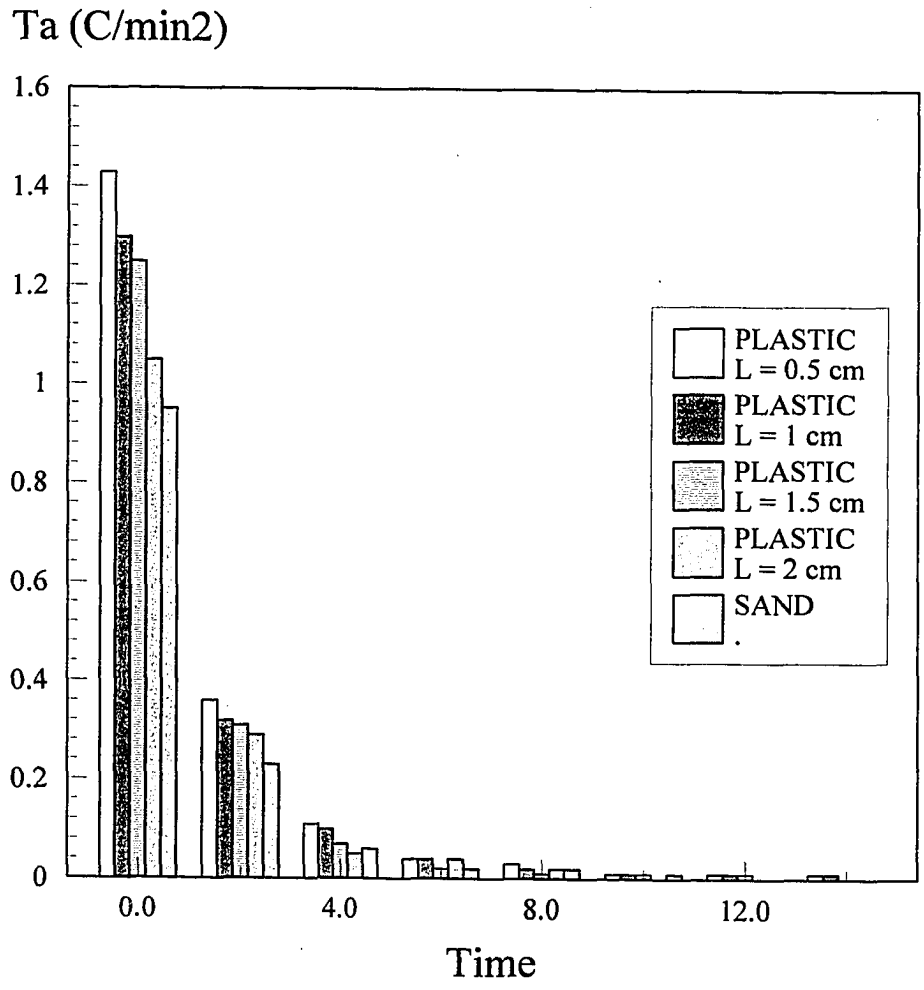


Figure 2-26
The acceleration of surface temperature changes in the vicinity of a plastic object buried under sand at depth L=0.5 cm, 1 cm, 1.5 cm and 2 cm and the sand-only area, in the first 20 minutes when radiation switched off.

flux on the surface of ground. The value of the object's related flux was decided by the statistical results of the indoor experiments. The results of the modified mathematical model were compared to the experiments. The mathematical model could be used in later studies of the properties of thermal images of the surface of ground to detect the buried objects. Some more experiments need to be done to further verify the object's related flux.

For the finite size buried objects, the temperature distribution on the surface of the ground provides the information of the shape of the objects and their buried depth. Mathematical calculations were carried out, by solving the temperature distribution differential equations, and the isothermal contours were drawn. As the thermal properties of the surface of ground are affected differently by the objects' composition, size, and depth, the heat conduction and the rate of temperature transference on the surface will also be different. The resulting isothermal contours from the calculation could be very helpful to detect and identify a buried object.

With such a mathematical model, we can theoretically analyze the characteristic of the surface temperature and study the behavior of temperature chances of the surface. A database can be set up with the thermal properties of the ground with different objects buried at different depth. With this theoretic data, we can training a recognition system to detect the buried objects automatically in the future.

Further detection enhancement can be done by processing the infrared images and the data taken from the infrared images.

The processing of infrared images by subtraction the heating cycle's image from the cooling cycle's image can emphasis the shape of the object and de-emphasize the non-uniformity of the sand.

Along with observing the surface temperature, calculating the temperature differences between the buried objects and the sand surface, and the speed and acceleration of temperature changes will enhance the real time detection.

## 3.6 Reference


[1] J. C. Jaeger, "Conduction of Heat in a Solid with Periodic Boundary Conditions, with Application to the Surface Temperature of the Moon", Proceeding Cambridge Phil. Society, 49 (2),355-359, 1953.

[2] Anne B. Kahle, "A Simple Thermal Model of the Earth's Surface for Geologic Mapping by Remote Sensing", Journal of Geophysical Research, Vol. 82, No.11, pp.1673-1680, April, 1977.

[3] Robert D. Watson, Brief Reports: "Surface-Coating Effects in Remote Sensing Measurements", Journal of Geophysical Research, Vol.75, No. 2, pp.480-484, January, 1970.

[4] Arthur E. Bymes and John R. Schott, "Correction of Thermal Imagery for Atmospheric Effects Using Aircraft Measurement and Atmospheric Modeling Techniques", Applied Optics, Vol. 25, No. 15, pp. 2563-2570, August 1986.

[5] G. N. Watson, "Theory of Bessel Functions (A Treatise on the Theory of Bessel Functions)", 1943.

[6] Ingersoll, "Heat Conduction With Engineering", 1954.

[7] P. Concus, D. Caseate, G. Jaehning, "Tables for the Evaluation of $\int x^{\beta} e^{-x}(x)dx$ by Gauss-Lager Quadrature", Math. Computation, 17 (83), pp. 245-250, 1963.

[8] Kenneth Watson, L.P. Roan, T.V. Affiliate, "Application of Thermal Modeling in the Geologic Interpretation of IR Images", International Symposium on Remote Sensing of Environment Proceedings 8th, V.2. pp.1237, 1972.

[9] Kenneth Watson, L.P. Roan, T.V. Affiliate, "Application of Thermal Modeling in the Geologic Interpretation of IR Images", International Symposium on Remote Sensing of Environment Proceedings 7th, V.3 pp.2017-2041, 1971.

[10] Kenneth Watson, "Periodic Heating of a Layer over a Semi-Infinite Solid", Journal of Geophysical Research Vol. 78, No. 26, pp.5904-5910, September 1973.

[11] Charles Alice, "Introduction to the Physics and Techniques of Remote Sensing", Wiley Series in Remote Sensing.

[12] H. S. Carslaw, J. C. Jagger, "Conduction of Heat in Solids", Second edition, Oxford at the Clarendon Press.

[13] Kenneth Watson, "Geologic Applications of Thermal Infrared Images", proceedings of the IEEE, Vol. 63, pp.128-136, January, 1975.

[14] A. H. Stroud, D. H Secrest, " Gaussian Quadrature Formulas", Prentice - Hall, Englewood Cliffs, NJ 1966.

[15] F. B. Hidebrand, " Introduction to Numerical Analysis", McGraw-Hill, New York, 1956.

[16] V. I. Krylov, "Approximate Calculation of Integral", Macmillan, New York, 1962.

# IV. CONCLUSIONS AND FURTHER WORK

## Conclusions and Further Work

The objective of the work was to develop mathematical models that would simulate and explain the thermal characteristic of the surface of the ground with and without a buried object when the flux on the surface was radiated by either a diurnal solar cycle heating source or an artificial step function heating source. The finite size of the buried objects must taken into consideration when calculating the temperature distribution on the surface. Based on the theoretical study, an infrared image detecting system was set up using an Informatric Model 740 infrared camera. The experiments tested the surface temperature with different material objects buried at different depths using an artificial radiation source (heating and cooling), as well as a diurnal solar radiation source. Further image and data processing to enhace the detection were discussed.

We concluded that there are two distinct possible modes of infrared detection:

One is the short-term step function heating and cooling of the surface which can be used to generate various rates of temperature changes on the surface depending on the materials buried under the surface. An technique that generates images of the rates of changes of the temperature image output from the camera can then be used to track the motion of isothermal contours and thus locate and indentify the buried objects. From our study and observations, this process will take several minutes.

The other mode is the long-term observation of surface temperature changes at a few selected times during the diurnal sunlight cycle which allows for the generation of images based on temperature differences as they present the sum of the average heating and cooling rates.

Together with the above thermal methods, geometrical means of object recognition based on regularity of shapes can be employed to indentify buried objects. To this end, work is in progress in image processing and recognition techniques to isolate areas on the sand surface with regular temperature contours, then track thermal changes, and speed and acceleration of temperature changes in such areas.

Since thermal infrared detection capabilities can be significantly enhanced by incorporating of the surface rate of temperature change information into a detection scheme along with conventional analysis of the geometric temperature distribution at a particular point during heating or cooling (via diurnal solar or artificial irradiation), the further work of image analysis and data procession will be expected to collect and abstruct more information of the thermal property of the surface of the ground. An image recognition routine will be developed based on the information of the contour the areas of interest, comparing the image contours to the known shape of the buried object for geometric discrimination.

# V. APPENDIX

# Appendix

5.1 Thermal properties of some material

| Materiel | K Cal/m/sec/ | ρ Kg/m3 | C Cal/Kg/C | k m2/sec | P Cal/m2/C/s |
|---|---|---|---|---|---|
| Aluminum | 0.48 | 3.7 | 0.206 | 0.48 | 0.517 |
| Cast iron | 0.12 | 7.4 | 0.136 | 0.12 | 0.3475 |
| Dry sand | 0.00063 | 1.65 | 0.19 | 0.0020 | 0.01405 |
| Avg. rock | 0.0042 | .. | .. | 0.0118 | 0.03866 |
| Plastic | 0.0055 | 0.41 | 0.30 | 0.0045 | 0.00823 |

5.2 Computer programs

CALCULATION OF SURFACE TEMPERATURE AND DISTRIBUTION

Program **STF**:

Function: Calculate surface temperature of semi-infinite object with solar radiation Equation ( 1.3 ) through equation ( 1.10 ).

Including files: stf.c, stc.c, stwmd1.c, stwmd2.c, stflux.c, stcalt.c, strop.c

Head files: stsunm.h, stsun.h, stcdm.h, stcd.h

Input data files: ahdat.dat, stw20.dat, stw24.dat, stw5.dat, stw480.dat, stw720.dat

Output files: stow**, stoflu**, stomp**, stod**

Program **STFEXP**:

Function: Calculate surface temperature of semi-infinite object with step function radiation. Including files: stfexp.c, stcexp.c, stwmdexp.c, stcaltexp.c, strop.c

Head files: stsunm.h, stsun.h, stcdmexp.h, stcdexp.h

Input data files: ahdat.dat, stw20.dat, stw24.dat, stw5.dat, stw480.dat, stw720.dat

Output files: stow**, stoflu**, stomp**, stod**

Program **STFNEW**:

Function: Calculate surface temperature of semi-infinite object with solar radiation. Equation (1.3) through equation (1.7), and step function flux on the surface by inputing the name of objects buried and soil and give the depth of buried and size of the object. It will use the data-base of thermal properties of objects.

Including files: stfnew.c, stnewwmd1.c, stflux.c, stcalt.c, strop.c

Head files: stsunm.h, stsun.h, stcdm.h, stcd.h

Input data files: ahdat.dat, stw20.dat, stw24.dat, stw5.dat, stw480.dat, stw720.dat

Output files: stow**, stoflu**, stomp**, stod**

Program **STMDB**:

Function: Generate the data-base of thermal property of materials. The data file it creates is: STMDB.dat and THERMALP.dat.

Program **STDISIN**:

Function: Calculate the integral value for surface temperature distribution with finite cylindrical object buried underground. It finds the soil and material from the data-base

"THERMALP.dat" by name "soil/material", the distance of buried L and the size in depth of buried material D. Then it calculates the integral for Ve and V1 in equations (2.3) through equation (2.10).

Program **STMFN**:

Function: Managing the name of all ST files by given name of soil and material and the depth of L, the wide of D, the radius A and the emissivity of em. It also calculates temperature distribution by given local time and observation time.

## 5.3 Thermal infrared camera Model 740

Model 740 thermal infrared imaging camera is from Inframetrics Inc. It has four primary subsystems: Optical Image Data Generation, Image Processing, System Control and Image Output. Figure C shows Inframetrics Model 740 Infrared Imaging Radiometer System Plot.

The camera incorporates a HgCdTe detector sensitive in the long-wave range (8 to 12 micrometer wavelength), cooled to $77^{o}$ k via a unique ultra-compact closed cycle cryogenic refrigerator, eliminating the need for cryogen. The field of view (20 deg. H x 15 deg. V, using a 1X lens) is scanned by the detector at the resolution of 1.8 milliradians, with the display resolution of 256 Horizontal by 400 Vertical at the standard TV frame rate of 30 Hz. The temperature resolution of the camera is specified at 0.1 $^{0}$C (at 30 $^{0}$C). the sensitivity is further enhanced by the addition of a real-time frame

averaging feature to the standard Model 740 configuration, improving the signal-to-noise ratio by as much as a factor of four.

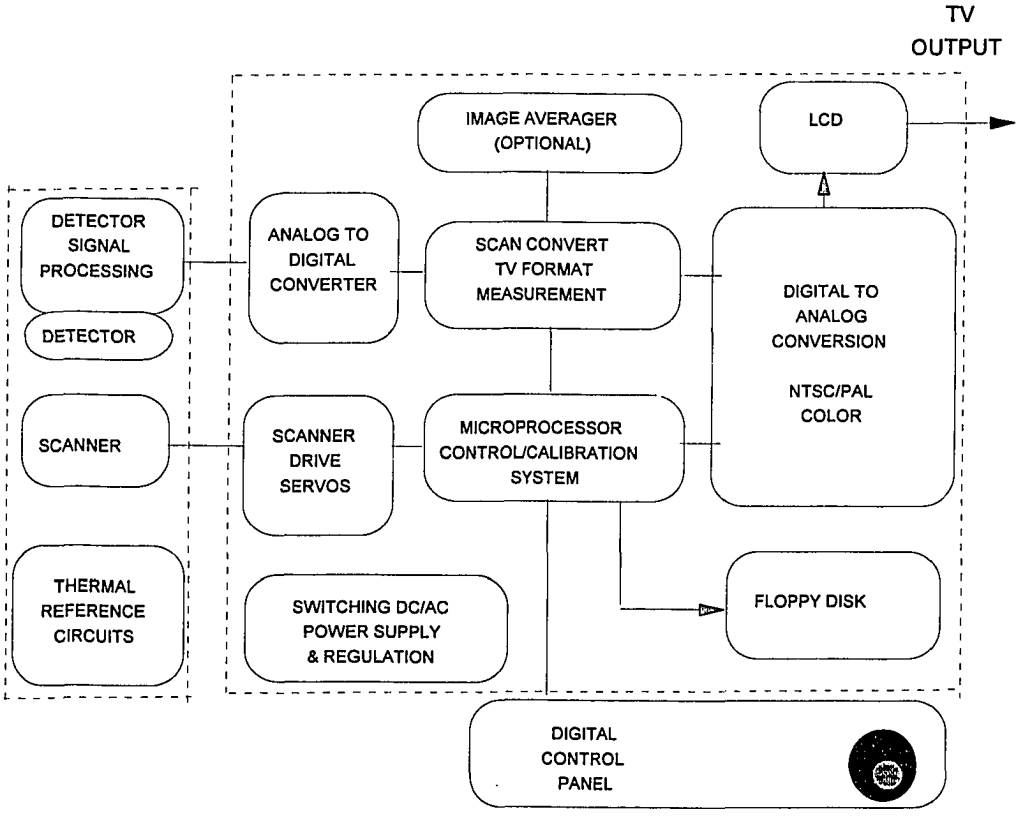


Figure 5-1

The Model 740 control/electronics unit contains circuits to process, digitize, and reformat the infrared signal for display in color or black and white on the LCD or external video monitor. A microprocessor performs internal calibration as the scanner temperature changes, lenses are installed, or settings are altered by the operator. The microprocessor accesses individual picture elements, then calculates temperatures using calibration tables corresponding to the optical filter/lens combination in use. A pulse-width modulated

switching power supply accepts a wide range of DC input voltage with excellent noise immunity. The control/electronics unit is in the camera controller which connects to the detector head via a cable. Additionally the camera controller has a 4-5" floppy disk drive that can digitally store up to 25 thermal images per diskette as TIFF files. The controller also incorporates a 4" color LCD monitor for display of live or stored images in 8 bit ( or less ) gray level or pseudo color. It also incorporates a standard video output which allows for display of live or stored images on a larger monitor, real time recording of images on a VCR recorder, and real time digitization and storage of images into a computer via a frame grabber.

# VI. BIBLIOGRAPHY

## Bibliography

[1] Aamodt, L. C. , Maclachlan Spiecer, J, W., and J. C. Murphy, "Analysis of Characteristic Thermal Transit Times for Time-Resolved Infrared Radiometry Studies of Multilayered Coatings", J. Appl. Phys. 68, pp 6087-6098 (1990).

[2] Alice, Charles "Introduction to the Physics and Techniques of Remote Sensing", Wiley Series in Remote Sensing.

[3] Boulton, Herb and Blaes, Maurice, "Thermal Image Generation and Analysis", E E Evaluation Engineering, January, 1986.

[4] Bymes, Arthur E. and Schott, John R., "Correction of Thermal Imagery for Atmospheric Effects Using Aircraft Measurement and Atmospheric Modeling Techniques", Applied Optics, Vol. 25, No. 15, pp. 2563-2570, August 1986.

[5] Carslaw, H. S. and Jagger, J. C., "Conduction of Heat in Solids", Second edition, Oxford at the Clarendon Press.

[6] Carts, S. L.Jr., "Feasibility of Land Mine Detection by Infrared Thermal Imaging," Report RR-1744, Fort Belvoir, Va., USAERDL, 25 March 1963.

[7] Cielo, P. "Pulsed Photothermal Evaluation of Layered Materials", J. Appl. Phys. 56, PP 230-234 (1984).

[8] Clark,Brenda M., "Keeping an Eye on Hot Spots", Circuits Manufacturing, December, 1985.

[9] Concus, P., Caseate, D. and Jaehning, G., "Tables for the Evaluation of $\int x^{\beta} e^{-x}(x)dx$ by Gauss-Lager Quadrature", Math. Computation, 17 (83), pp. 245-250, 1963.

[10] Danaher, Hugh, "Thermography, Understanding the Expanded Role of Thermal Images in Production Testing", E E Evaluation Engineering, December, 1988.

[11] Danaher, Hugh, "Thermal Images Show Hybrids' Defects", Electronic Packaging & Production, September, 1986.

[12] Duggin, Micheal J., "Discrimination of Targets from Background of Similar Temperature, Using Two-Channel Data in the 3.4-3.1 μm and 11-12 μm Regions", Applied Optics Vol. 25, No. 7, pp. 1186-1195, April 1986.

[13] Elvidge, Christopher D., "Thermal Infrared Reflectance of Dry Plant Materials: 2.5-20.0 μm", Remote Sensing of Environment 26, pp.265-285, 1988.

[14] Favro, L. D., Jin H. J., Kuo P. K., Thomas, R. L. and Wang, Y. X. "Real Time Thermal Wave Tomography", in Photoacoustic and Photothermal Phenomena II, Springer Series in Optical Sciences, Vol 69, pp519-521 (Springer-Verlag 1992).

[15] Gravitte, Dwight L., "Field Evaluation of Hand-Held Thermal Viewer for Mine Detection," Report 2022, Fort Belvoir, Va., USAMERDC, February 1972.

[16] Gravitte, Dwight L., "Potentials and Limitations of Thermal Images for Mine Detection," Report 2172, Fort Belvoir, Va., USAMERDC, April 1976.

[17] Groningen, Wiely D. H. Van, Vermeij, G. F., "Geometric Reconstruction of Buried Heat Sources from a Surface Thermogram", IEEE Transactions on Pattern Analysis and Machine Intelligence, Vol. PAM-7, NO. 5, pp.610-616, September 1985.

[18] Hidebrand, F. B., "Introduction to Numerical Analysis", McGraw-Hill, New York, 1956.

[19] Hudson, Richard D., and Hudson, Jacqueline W., "The Military Applications of Remote Sensing by Infrared", Proceedings of the IEEE, Vol. 63, pp.105-127, January, 1975.

[20] Ingersoll, "Heat Conduction With Engineering", 1954.

[21] Jaeger, J. C., "Conduction of Heat in a Solid with Periodic Boundary Conditions, with Application to the Surface Temperature of the Moon", Proceeding Cambridge Phil. Society, 49 (2),355-359, 1953.

[22] Jakob, "Heat Transfer".

[23] Kahle, Anne B., "A Simple Thermal Model of the Earth's Surface for Geologic Mapping by Remote Sensing", Journal of Geophysical Research, Vol. 82, No.11, pp.1673-1680, April, 1977.

[24] Keller, Harry and Nawrocki, Edmund, "Evaluation of Thermal Viewers for Mine Detection," Report 2526, Fort Belvoir, Va., USABRDC, May 1992.

[25] Krylov, V. I., "Approximate Calculation of Integral", Macmillan, New York, 1962.

[26] Lau, S. K., Almond, D. P., and Patel, P. M., "A Qauntitative Analysis of Pulsed video Thermograghic imaging of subsurface defects", in Photoacoustic and Photothermal Phenomena II, Springer Series in Optical Sciences, Vol 69, pp522-524 (Springer-Verlag 1992).

[27] Lyon, R. J. P. and Burns, Eugene A., "Analysis of Rocks and Minerals by Reflected Infrared Radiation", Economic Geology, Vol. 58, 1963, pp. 274-284, 1963.

[28] Nolan, R. V. and Egghart, H.C., "Meradcom Mine Detection Program: 1960-1980," Report 2294, Fort Belvoir, Va., USAMERDC, March 1980.

[29] Stout, Arthur, "IR Images Track Heat Sources To Make Things Smart", R & D Magazine, February, 1992.

[30] Stroud, A. H. and Secrest, D. H., "Gaussian Quadrature Formulas", Prentice - Hall, Englewood Cliffs, NJ 1966.

[31] Vincent, Robert K., "The Potential Role of Thermal Infrared Multi-spectral Scanners in Geological Remote Sensing", Proceedings of the IEEE, Vol. 63, pp.137-147, January, 1975.

[32] Watson, G. N., "Theory of Bessel Functions (A Treatise on the Theory of Bessel Functions)", 1943.

[33] Watson, Kenneth, "Geologic Applications of Thermal Infrared Images", Proceedings of the IEEE, Vol. 63, pp.128-136, January, 1975.

[34] Watson, Kenneth, "Periodic Heating of a Layer Over a Semi-Infinite Solid", Journal of Geophysical Research Vol. 78, No. 26, pp.5904-5910, September 1973.

[35] Watson, Kenneth, Roan, L.P. and Affiliate, T.V., "Application of Thermal Modeling in the Geologic Interpretation of IR Images", International Symposium on Remote Sensing of Environment Proceedings 8th, V.2. pp.1237, 1972.

[36] Watson, Kenneth, Roan, L.P. and Affiliate, T.V., "Application of Thermal Modeling in the Geologic Interpretation of IR Images", International Symposium on Remote Sensing of Environment Proceedings 7th, V.3 pp.2017-2041, 1971.

[37] Watson, Robert D., Brief Reports: "Surface-Coating Effects in Remote Sensing Measuments", Journal of Geophysical Research, Vol.75, No. 2, pp.480-484, January, 1970.

[38] IR Imaging Radiometer, Inframetrics Model 740, "User's Menu".

[39] IIT Research Institute, "Dragon Wagon--Feasibility Study of Land-mine Thermal Signature Enhancement," Report TR-90 (6179)-1, Fort Belvoir, Va., USAMERDC, February, 1990.